JOURNAL OF GEOPHYSICAL RESEARCH, VOL. 106, NO. B1, PAGES 683–702, JANUARY 10, 2001

A theoretical model of hotspot volcanism: Control on volcanic spacing and patterns via magma dynamics and lithospheric stresses

Christoph F. Hieronymus

Danish Lithosphere Centre, Copenhagen, Denmark

David Bercovici

Department of Geology and Geophysics, University of Hawaii at Manoa, Honolulu, Hawaii

Abstract. Many linear island chains are thought to be the result of the steady motion of the lithospheric plates over stationary hotspots. The occurrence of discrete, nearly regularly spaced volcanoes, rather than continuous ridges, are assumed to be caused by the interaction of flexural stresses (due to the volcanic loads) with magma percolation. A parameter study is performed on a simple model that incorporates these effects in addition to dike wall erosion. It is demonstrated that the strength of the erosional feedback determines whether the model generates discrete volcanoes or a continuous ridge. The intervolcanic spacing depends not only on the elastic thickness of the lithosphere but also on the magma pressure at the base of the lithosphere. The size of the eruptive region of the individual volcanoes is controlled by the elastic response of the lithosphere to magma overpressurization. If an initial off-axis edifice is introduced, the model is able to preserve this asymmetry and produce an alternating series of volcanoes. A small initial perturbation grows over time, resulting in double lines or wider patterns depending on the width of the magma source region. Single lines of volcanoes therefore indicate very narrow magma source regions.

1. Introduction

Perhaps the most striking feature of hotspot tracks, aside from a frequently observed linearity due to constant plate motion over a stationary magma source, is the regular spacing of the individual shield volcanoes [*Vogt*, 1974]. This periodic spacing may be caused by a regular oscillation in the magma supply at the base of the lithosphere or by magma-lithosphere interaction.

Variability in the magma supply has been proposed to be due to oscillations in the plume source caused by solitary waves [*Scott et al.*, 1986; *Olson and Christensen*, 1986; *Schubert et al.*, 1989; *Helfrich and Whitehead*, 1990] or diapiric instability of plumes tilted by mantle shear flow [*Skilbeck and Whitehead*, 1978; *Whitehead*, 1982; *Olson and Singer*, 1985]. However, models based on fluctuations in the plume source predict volcanic spacing that increases with plate velocity. This is not observed; instead, the spacing has been shown to correlate with lithospheric thickness [*ten Brink*, 1991], an observation that is difficult to reconcile with models of volcano formation by plume instability.

Aside from explaining the equidistant spacing of shield volcanoes, a complete model of magma transport at intraplate locations also has to take into consideration (1) the high ascent velocities of magma through the lithosphere, of the order of meters per second [*Carmichael et al.*, 1977; *Spera*, 1980]; (2) the problem of magma solidification as it traverses tens of kilometers through a relatively cool lithosphere [*Turcotte*, 1981]; and (3) compressive lithospheric flexural stresses due to large volcanic loads, which should preclude the existence of magma-filled voids and pathways and thus inhibit the formation of large volcanoes in the first place.

Paper number 2000JB900355.
0148-0227/01/2000JB900355$09.00

1.1. Magma Flow Mechanisms

Various hypotheses have been forwarded for the mechanism of magma migration through the lithosphere at intraplate locations. A simple physical model which was developed for island arc volcanics is the diapiric model [*Marsh*, 1978] in which mantle material is transported upward through the viscous mantle via a conduit, and the lithosphere is modeled as a viscous medium through which pockets of melt ascend. This approach, however, necessitates representing the lithosphere as a fluid with unrealistically low viscosity in order to obtain reasonable diapir ascent times. Another possibility is that dikes form at locations of weakness in the lithosphere. *Vogt* [1974] suggests that hotspot volcanoes lie at the intersections of joints, which may have preexisted in the lithosphere or have been caused by stresses associated with the hotspot itself. Such joints would preferen-

tially form with a regular spacing aproximately equal to the thickness of the lithosphere, thus explaining the equidistant spacing of volcanic shields in hotspot tracks. *Vogt* [1974] does not address the actual mechanism of magma transport, such as the physics of fracture formation at points of weakness. The main problem with the model of magma flow at joint intersections is that the observed directions of en echelon lines of volcanoes in a given hotspot province do not appear to be congruent in general with the directions of regional tectonic or local plume-generated stresses nor with the directions of obvious locations of lithospheric weakness such as transform and normal faults [*Vogt*, 1974].

An alternate approach focuses on the dynamics of crack propagation in an elastic medium [*Lister and Kerr*, 1991; *Lister*, 1990; *Spence et al.*, 1987; *Turcotte*, 1982, 1981]. Generally, magma-filled fractures are assumed to propagate upward through a homogeneous lithosphere, driven by the differential buoyancy of the melt. Flow through cracks provides the high flow speeds evidenced by the existence of sizeable xenoliths [*Spera*, 1980; *Carmichael et al.*, 1977]. Solidification of magma along the fracture walls is believed to quickly shut off the flow until a new fracture forms, resulting in the observed episodicity of surface eruptions. However, it is not clear that this model could display long-term periodicity, which would result in the formation of discrete volcanoes with spacing proportional to lithospheric thickness.

Indeed, another possible mechanism for magma flow at hotspots has been implicitly suggested by *ten Brink* [1991], who demonstrated a strong correlation between lithospheric thickness and volcano spacing in various volcanic regimes, including hotspots. His conclusion is that the flow mechanism must be dependent on the in-plane stresses caused by the downward flexure of the lithosphere underneath volcanic edifices. The present model builds on this idea; magma transport through dikes with elastic displacement of the dike walls in response to changes in fluid pressure and the general stress regime provides a feasible process that takes into account the effect of flexural stresses.

1.2. Melting and Erosion of Fracture Walls

The potentially important process of melting of the dike walls, or "melt-back," has been largely neglected or underestimated in many previous studies. The possibility of melt-back for surface fissures has been investigated for a simple model of a single mineral phase [*Bruce and Huppert*, 1990; *Lister and Dellar*, 1996]. *Bruce and Huppert* [1990] argue that earlier models of magma flow through dikes overestimate the amount of solidification because they neglect (1) the effects of heat advection in the magma and its influence on the temperature profile in the surrounding solid [*Delaney and Pollard*, 1982] and (2) the effect of latent heat release on solidification. Including these terms in the calculations, it was found that magma-transporting fractures of width greater than a critical value may remain open or grow in width over an indefinite period of time as long as the driving magma pressure gradient is maintained [*Bruce and Huppert*, 1990; *Lister and Dellar*, 1996].

1.3. Coupling Flow Through Fractures With Melting and Erosion

Kelemen and Aharonov [1998] proposed a simple model for flow of magma from a magma chamber to the surface at mid-ocean ridges, accounting for flow through fractures, elastic stresses of the country rock, and solidification of magma within the dike. The magma chamber was approximated as a pressurized melt lens with a constant magma influx that causes the chamber to inflate against the surrounding elastic stresses. The magma pathway to the surface was assumed to be a dike which changes in width depending on the difference between magma pressure and elastic stresses and may be constricted by magma solidification if the flow rate drops below a critical value. The model was found to be able to explain both the periodic formation of magma fractures and the generation of layered gabbros in the lower crust beneath oceanic spreading ridges.

On a larger scale in both space and time, the process of fracture of an elastic medium under the influence of flexural stresses, combined with melt-back and other erosion mechanisms of the conduit walls, has been shown to generate discrete hotspot volcanoes with realistic spacing [*Hieronymus and Bercovici*, 1999]. In this model, which is investigated in detail in the present study, a homogeneous lithosphere overrides a stationary hotspot of constant flux; thus any time dependence observed at the surface is due to the interaction of magma and lithosphere. Given the complex dynamics of the model, however, the results depend on a large number of parameters. Some of these parameters, such as the densities of magma, lithosphere, and asthenosphere are assumed known, while others (such as the parameter controlling the effect of conduit wall erosion) are difficult to constrain. In spite of the large number of degrees of freedom of the model, it will be shown that the results are characterized by two possible modes: discrete volcanoes or a continuous ridge. Only for extreme parameter values is there a third mode in which the entire lithosphere becomes permeable to magma flow.

For the model depending solely on flexural stresses [*ten Brink*, 1991] it was assumed that the volcanic spacing is equal to the distance from the center of a volcanic load (which was approximated as a point load) out to the radius of the zero crossing of the flexural stresses, which was shown to depend on the elastic characteristics and the thickness of the lithosphere but not on the amplitude of the volcanic load. In the present model this simple relationship no longer holds as the flexural stresses interact with other stresses as well as with the effect of conduit erosion. Since the determination of the elastic lithospheric thickness is independent of the observations of volcano spacing, this value, along with the observed relation between volcano spacing λ and lithospheric thickness H may be used to constrain the model parameters.

2. Theory

The physical processes relevant for the flow of magma through the lithosphere at intraplate locations operate on greatly varying timescales and length scales. While a given shield volcano and the corresponding flexure and flexural

stresses grow over timescales of 10^6 years, with length scales of the order of 10–100 km, a typical dike that acts as a magma channel is of the order of 1–10 m wide and one to several kilometers long and is typically formed over a timescale of days [*Lister and Kerr*, 1991]. A practical approach to this problem was introduced by defining the permeability of the lithosphere as a field variable [*Hieronymus and Bercovici*, 1999]. Neglecting the small-scale structure of cracks, the presence of one or more fractures is represented by a high-permeability region, which may be seen as an average in both space and time, while the background state of the lithosphere is impermeable. The permeability will be assumed to depend on the stress regime in the lithosphere, on the fluid pressure, and on the process of remelting and erosion of the fracture walls if the magma flux is sufficient.

The physics of fracture formation and of dike wall melting have been the subject of numerous studies [*Rubin*, 1995; *Lister and Dellar*, 1996]. In the present model, dikes are assumed to form as soon as the magma pressure is greater than the sum of the local stresses and the tensile strength of the lithosphere. The more complex physics occurring near the dike tip, and the fluid dynamical and thermomechanical effects of the magma during fracture propagation, do not enter the problem explicitly. Once a dike has been formed, its thickness and thus its ability to transport magma have been shown to depend on the difference of magma pressure and the normal stresses in the surrounding rock [*Rubin*, 1995]. Additional dike opening is assumed to be provided directly by the removal of wall rock from both melting and erosion, which are controlled by inputs of heat and mechanical energy.

Without tectonic background stresses a flexed homogeneous lithospheric plate, subject to deflections that are small in comparison with the thickness, has a region of zero volume change at middepth [*Timoshenko and Woinowsky-Krieger*, 1959], while the rock above and below is extended or compressed, depending on the sign of curvature (see Figure 1). Tensile flexural stresses near the surface of the lithosphere are therefore always accompanied by compressive stresses near the base, and vice versa. Since the excess magma pressure and buoyancy of the melt are largely balanced dynamically by viscous flow within the dike [*Spence and Turcotte*, 1985], formation of new dikes in the lithosphere by hydraulic fracture is only possible in regions of tensile or low compressive stresses. In order for magma to penetrate vertically through the entire thickness of the lithosphere the stress regime must not be strongly compressive anywhere in its path. In other words, new dikes can only form in regions of minor flexural plate curvature. A complete model of magma transport at intraplate locations should take into account the lithospheric stresses at all depths. In this simplified model the lithosphere will be modeled in the two horizontal dimensions by thin plate theory, implicitly assuming that the stresses vary linearly with depth; the stresses are thus maximum at the top and bottom boundary of the lithosphere. Only the stresses near the surface will be considered, as this is where fracturing is most likely to occur [*Kohlstedt et al.*, 1995; *Evans and Kohlstedt*, 1995]. Closer to the base of the lithosphere, the rock is probably more viscous rather than elastic and may not fail by brittle fracture. Studies of porous viscoelastic media [*Connolly and Podladchikov*, 1998] are beginning to shed some light on the mode of melt transport in the transition zone from viscous mantle to elastic, brittle lithosphere, but it is not clear how imposed stresses affect the flow. Moreover, given that the rheology of the lithosphere changes with depth, the flexure of the lithospheric plate is likely a mixed mode of viscous and elastic deformation [*Schmalholz and Podladchikov*, 1999], and elastic thin-plate theory may not accurately describe the stress field at depth. While the appropriate magma transport mechanism in this regime is thus not known, observations of volcanism on top of the flexural bulge [*Clague et al.*, 1990] seem to indicate that the compressive flexural stresses at depth do not significantly inhibit magma flow through the lithosphere.

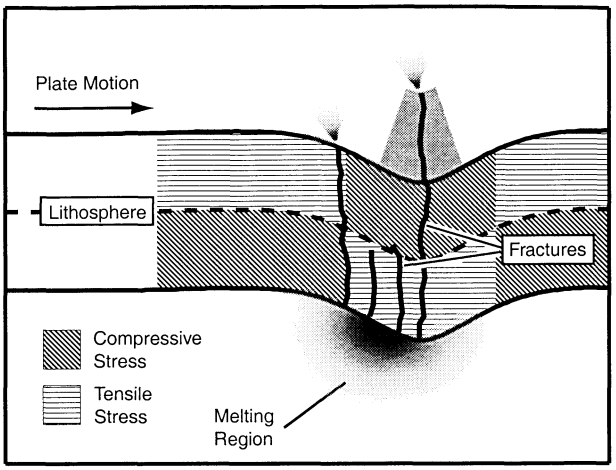

Figure 1. Illustration of flexural stresses in the lithosphere. Magma fractures form where melt is available at the base of the lithosphere and propagate upward as long as the magma pressure is greater than the compressive local stresses in the host rock. Magma overpressurization is low [*Maaløe*, 1998] because the magma buoyancy is largely balanced by viscous flow [*Spence and Turcotte*, 1985]; hence fractures only form where flexural stresses are tensile or near zero. The flexural stresses are greatest near the top and bottom boundaries of the lithosphere. Once a magma pathway is established, the fracture is kept open in an environment of increasing flexural stresses by erosion of the fracture walls.

The effect of the hotspot is prescribed in the model as a radially symmetric tensile stress region. This stress may be the result of plume material spreading radially outward underneath the lithosphere, or a high magma pressure relative to the asthenosphere, forcing open fractures and cracks. In order to maintain some control over the shape of the plume stress as well as over its amplitude and width, we parameterize the stress using a "super-Gaussian" function [*Wessel*, 1993], which is defined as $\exp[-(x/x_0)^{2p}]$, where x is the position from the center of the super-Gaussian shape, and x_0 is its halfwidth. The parameter p determines the shape of the super-Gaussian function: For p=1, the function is a

Table 1. Dimensional Parameters

Parameter	Description	Value
A	amplitude of plume stress	Pa
B	constant	—
c	specific heat	J (kg °C)$^{-1}$
C, C_o	constants	Pa
D	flexural rigidity	Pa m^3
E	Young's modulus	Pa
f	porosity	—
g	gravitational acceleration	m s^{-2}
h	height of volcano	m
H	thickness of lithosphere	m
k, k_o	permeability	m^2
L	latent heat of melting	J kg^{-1}
P	dynamic pressure	Pa
r	radius of source stress	m
T_m	temperature of melt	°C
T_w	temperature at wall	°C
T_∞	far field temperature in solid	°C
v	lithospheric plate velocity	cm yr^{-1}
V	Darcy velocity of magma	m s^{-1}
w	flexural displacement	m
ΔQ	change in magmatic energy	J m^{-3}
ε	energy content per volume of magma	J m^{-3}
μ	dynamic viscosity of magma	Pa s
ν	Poisson's ratio	—
ρ_a	density of asthenosphere	kg m^{-3}
ρ_l	density of lithosphere	kg m^{-3}
ρ_m	density of melt	kg m^{-3}
ρ_w	density of water	kg m^{-3}
σ_1	tensile strength of lithosphere	Pa
σ_f	flexural stress	Pa
σ_o	background stress in lithosphere	Pa
σ_p	plume stress	Pa

simple Gaussian function, while for values >1, the shape becomes increasingly more flat-topped with steeper flanks. The model is placed in the frame of reference of a leftward moving lithospheric plate and thus the super-Gaussian shaped plume propagates in the positive x direction with respect to the lithosphere; hence the tensile stress of the source is defined by

$$\sigma_p(x,y,t) = Ae^{-\left[\frac{(x-vt)^2+y^2}{r^2}\right]^p} - \sigma_o\ , \qquad (1)$$

where A is the amplitude and r is the half width of the source (see Table 1 for a list of parameters). The stress σ_o represents the combined effects of a lithospheric background stress and an asthenospheric underpressurization relative to the plume. A plausible interpretation of this underpressurization is the "viscous head loss" of the asthenospheric material due to its higher viscosity with respect to the melt within the plume. Part of the stresses σ_p and σ_o may thus be an effective pressure due to the assumption of constant viscosity, and increased values of plume stress σ_p may be seen as a proxy for the availability of melt; this is investigated in more detail in Appendix A.

Additional horizontal stresses are provided by plate flexure, which is a function of the surface load [*Turcotte and Schubert*, 1982], as described by

$$D\nabla_h^4 w + (\rho_a - \rho_w)gw = -\rho_m gh. \qquad (2)$$

Both variables w and h are functions of x, y, and t, where w is the vertical deflection of the lithospheric plate and h is the height of a volcanic edifice of density ρ_m, which is taken to be the same as the density of liquid magma [cf. *Maaløe*, 1998]. The flexural rigidity D is defined in terms of Young's modulus E, Poisson's ratio ν, and the thickness of the lithosphere H as $D = EH^3/12(1-\nu^2)$. The densities of the asthenosphere and of water are given by ρ_a and ρ_w, respectively. The operator ∇_h^4 is the horizontal two-dimensional biharmonic operator, defined as $\nabla_h^4 = (\partial^2/\partial x^2 + \partial^2/\partial y^2)^2$. The effects of the basal load are assumed to be negligible because the plate curvature at the center of the swell due to the plume top is observationally inferred to be small [*Wessel*, 1993].

In analogy with elastoporous media theory [*Biot*, 1941] the permeability of the lithosphere is controlled by the sum of the horizontal flexural stresses, which is an invariant. The total horizontal stress in terms of the displacement w is

$$\sigma_f = -\frac{EH}{2(1-\nu^2)}\nabla_h^2 w. \qquad (3)$$

This formulation is slightly different than what would be predicted using fracture dynamics. Fractures form in a direction perpendicular to the most tensile stress, and during their evolution their thickness only depends on this stress; the thickness is thus independent of the other stresses. This means that fractures are more efficient in causing porosity in a regime of large deviatoric stresses. The porous media approach was mostly chosen for its simplicity; even a parameterized fracture mechanical approach requires decomposing the stress field at each point into its eigenvalues and then using the largest eigenvalue to control the porosity.

The magma flow itself is described by Darcy's law, $V = -k\Delta p/\mu H$, where V is the Darcy velocity and Δp is the pressure difference between the top and the bottom of the lithosphere. The permeability k is controlled by the net horizontal stress in the lithosphere and by melting and erosion along the path of the magma.

Bruce and Huppert [1990] demonstrated that for an instantaneously emplaced fracture and a pressurized melt region, flow through the fracture always begins with a transient cooling phase during which magma solidifies along the fracture walls, thus constricting the flow. For fractures less than a critical width solidification continues until the dike becomes blocked and the flow ceases. For fractures greater than the critical width the advected heat flux eventually begins to melt back the solidified magma or the surrounding country rock. The melting process then continues as long as the driving pressure is maintained, thus gradually increasing the flow of magma through the fissure. Melt-back of the fracture walls has been shown to be controlled by three nondimensional parameters S_m, S_∞, and α [*Bruce and Huppert*,

1990]. The Stefan numbers of the melt and the solid are $S_m = L/c(T_m - T_w)$ and $S_\infty = L/c(T_w - T_\infty)$, respectively, where L is the latent heat of melting, c is the specific heat, T_m is the temperature of the melt at the source, T_w is the temperature at the edge of the dike, and T_∞ is the far-field temperature in the country rock. The third parameter is defined as $\alpha = (\mu\kappa H^2/\Delta p b_i^4)^{1/3}$, where κ is the thermal diffusivity, Δp is the pressure drop along the dike, and b_i is the initial half width of the dike. *Bruce and Huppert* [1990] show that for values of $S_m = 22$ and $S_\infty = 1.05$, which may be taken as typical values for magma flow at hotspots through cold lithosphere, the value of α has to be < 0.032 in order for a dike not to become blocked by solidification. For a dike of length $H = 35$ km this requires the initial half width of the dike to be > 1.8 m. Once the lithosphere has been preheated by prior fractures, the minimum width b_i decreases significantly.

While melt-back of fracture walls is the easiest to quantify, there are other processes which affect the permeability of the lithosphere, such as mechanical ablation and chemical reactions. We assume that the influence of melting and erosion of fracture walls on permeability is controlled by the rate of influx and efflux of net energy due to magma injection. This energy nominally includes all forms of energy that contribute to erosion, e.g., heat (for melting and for thermal conditioning which facilitates erosion by softening the rock [*Lister and Dellar*, 1996; *Bruce and Huppert*, 1990]), gravitational potential energy, internal mechanical energy, kinetic energy (for mechanical erosion [*Davies*, 1994]), chemical potential energy (for reactive or hydrating effects [*Bonatti*, 1990; *Burnham*, 1979]), etc. Since the various erosional effects and their interactions are difficult to estimate, we combine all of these processes into one variable ε, representing the net energy content of the bulk medium (wall rock plus magma) per volume in excess of the far-field value.

Overall, we assume that stress and erosion affect permeability by changing the magma volume fraction (i.e., porosity) f due to dikes and cracks. Incremental changes in σ_p, σ_f, and ε thus cause incremental changes in f:

$$C\,df = B\,d\varepsilon + d\sigma_p + d\sigma_f\ , \tag{4}$$

where B is a constant and C is a hybrid parameter where C^{-1} describes the effectiveness of the stresses and energy input in changing the porosity. Clearly, negative values of porosity f as well as values of f greater than one are physically meaningless. Moreover, on the continuum mechanical (i.e., kilometer size) scale of the model, values of f near unity are equally unattainable. We therefore construct the function $C(f)$ of the form

$$C = \frac{C_o}{f(f_{\max} - f)}\ , \tag{5}$$

which limits the possible range of f to values between zero and $f_{\max}$ by making the value of C approach infinity as f approaches either of its bounds. At low values of f the inefficiency of stresses in changing porosity represents the resistance to complete closure of fractures or pore spaces because the rock matrix becomes stiffer [*Guéguen and Palciauskas*, 1994] and the remaining magma is difficult to squeeze out [*Stevenson*, 1982]. Melting and erosion are inefficient in widening magma pathways at low porosity because heat conduction away from the conduits becomes dominant. The existence of $f_{\max}$ and the large value of $C(f)$ as $f \to f_{\max}$ are more complex. A possible explanation is that near the disaggregation limit of the rock matrix, increases in stress and energy go into responses other than an increase in porosity, such as deforming or heating the magma. As the porosity approaches $f_{\max}$, less and less energy is partitioned into effecting further porosity increases. The value of $f_{\max}$ is assumed to be similar to the disaggregation limit of melts, i.e., $0.01 \le f_{\max} \le 0.1$. The existence of $f_{\max}$ is thus a physical property of the rock. Alternatively, $f_{\max}$ may be determined by the system's dynamics, where a limited magma supply rate from the melt reservoir of the plume restricts the total magma flux through the fractures and thus results in a maximum porosity. This explanation may be similar to *Kelemen and Aharonov*'s [1998] model of periodically formed magma fractures, where in the present model we neglect the high-frequency periodicity. While the first explanation is simpler and does not require any knowledge about the plume, the alternative explanation allows for the maximum magma flux to be determined by the plume characteristics. Whatever the underlying cause of the maximum porosity, the value of $f_{\max}$ does not need to be evaluated explicitly as it only occurs coupled to other parameters. Nonetheless, in section 4.3 an estimate of $f_{\max}$ is calculated using some simple scaling arguments. Moreover, the choice of the function $C(f)$ is not crucial to the model results. Relation (5) was chosen for its simplicity and its integrability, resulting in the hyperbolic tangent in the permeability law. Other functions $C(f)$, which approach zero as $f \to 0$ and $f \to f_{\max}$, yield similar results.

With the above choice of $C(f)$, equation (4) may be integrated to yield the function $f(\varepsilon, \sigma_f, \sigma_p)$. The flow of magma through the lithosphere is assumed to be governed by Darcy's law, $V = -k/\mu\nabla P$, where V is the flux per unit area (i.e., the Darcy velocity), k is the permeability, μ is the viscosity of the magma, and P is the driving pressure. With a linear dependence of permeability k on porosity f, the permeability may be written as

$$k = \frac{k_o f_{\max}}{2}\left[1 + \tanh\left(\frac{\sigma_p + \sigma_f - \sigma_1 + B\varepsilon}{2C_o/f_{\max}}\right)\right], \tag{6}$$

where k_o is a reference permeability and σ_1 is an integration constant representing the intrinsic tensile strength of the far-field lithosphere.

The height of the volcanic edifice grows according to the ejection rate of magma onto the surface:

$$\frac{\partial h}{\partial t} = V. \tag{7}$$

The outward spreading of the volcanic edifice due to gravity flow is not taken into account in this model. Changes in the energy content ε of the rock-magma system are primar-

ily controlled by the injection rate of magmatic net energy, which is also proportional to V:

$$\frac{\partial \varepsilon}{\partial t} = \frac{\Delta Q}{H} V, \tag{8}$$

where ΔQ is the drop in magmatic energy per volume across the lithosphere from bottom to top. A different time dependence of the energy input is explored in section 3.8.

In addition to describing the time evolutions of h and ε, equations (7) and (8) combined also provide the simple relation $\varepsilon = (\Delta Q/H)h$, where both the energy ε and height h are assumed to be zero at some time t. This relation may be used to eliminate the variable ε from (6).

The transport of magma through the lithosphere is assumed to be in a direction that is nearly vertical, with the pressure gradient driving the flow being determined by the buoyancy of the magma, the hydraulic head of the magma inside the volcanic edifice, and the flexural deflection of the lithosphere into the underlying asthenosphere. The complete Darcy flow law is then

$$V = \frac{k_o f_{\max}}{2\mu}\left[1+\tanh\left(\frac{\sigma_p+\sigma_f-\sigma_1+B\Delta Q h/H}{2C_o/f_{\max}}\right)\right] \times \left[(\rho_l-\rho_m)g-(\rho_m h+\rho_a w)\frac{g}{H}\right], \tag{9}$$

where ρ_l is the density of the lithosphere. If σ_p represents magma overpressurization rather instead of plume tensile stress, then, strictly speaking, it should be included in the driving pressure; however, this is found to have little significant effect on the final results.

Equations (1) to (3) and (7) to (9) may be combined into three equations and nondimensionalized using the following length scale, pressure scale, and timescale: $\hat{X} = [D/g(\rho_a - \rho_w)]^{1/4}$, $\hat{P} = \rho_l g H$, and $\hat{T} = \hat{X}/v$. The length scale is proportional to the flexural parameter and thus represents the wavelength of flexural displacement of the lithosphere. The pressure scale is equal to the lithospheric overburden, while the timescale is the time taken by the lithospheric plate to traverse the distance of one length scale. In this case, the dimensionless governing equations are

$$\frac{\partial h}{\partial t} = c_1\left[1+\tanh\left(c_2(\sigma_p-\nabla_h^2 w+c_4 h-c_5)\right)\right] \times (\gamma_2 - h - \gamma_1 w), \tag{10}$$

$$\nabla_h^4 w + w = \gamma_3 h, \tag{11}$$

$$\sigma_p = c_3 e^{-\frac{[(x-t)^2+y^2]^p}{c_6}}, \tag{12}$$

where the two constant pressures σ_o and σ_1 of (1) and (9) have been combined into c_5, and thus the nondimensional plume stress differs from the dimensional one by addition of a constant; see Table 2.

In the combined system of (10) to (12), the nonlinear character of the dynamical system is clearly seen. The magma flow is driven by a pressure gradient which is linearly dependent on the height h of the volcanic edifice. This flow is modified by the permeability which is a function of h itself. Moreover, it is noted that the melting and erosion mechanism ($c_4 h$) provides a positive feedback on the time evolution of h, while flexural stresses provide a negative feedback since the flexural deflection w is directly related to h by (11). Both feedback effects are of equal order, i.e., within the hyperbolic tangent function, both the flexural stresses and the melt-back effect depend linearly on h. This characteristic of the governing equations has important consequences for the dynamical behavior of the model. If, for example, the positive feedback due to melt-back is greater than the effect of the flexural stresses at low values of h, it then it will remain dominant for all values of h.

Table 2. Dimensionless Parameters

Parameter	Definition	Value
c_1	$\frac{k_0 f_{\max} g \rho_m}{2\mu v}\left(\frac{E}{12gH(\rho_a-\rho_w)(1-\nu^2)}\right)^{1/4}$	1.17
c_2	$\frac{f_{\max}}{4C_o}\left(\frac{12E^3 Hg(\rho_a-\rho_w)}{(1-\nu^2)^3}\right)^{1/4}$	varied
c_3	$\frac{2A(1-\nu^2)}{EH}\left(\frac{D}{g(\rho_a-\rho_w)}\right)^{1/4}$	varied
c_4	$2B\Delta Q\left(\frac{1-\nu^2}{12EHg(\rho_a-\rho_w)}\right)^{1/2}$	varied
c_5	$2(\sigma_o+\sigma_1)\left(\frac{(1-\nu^2)^3}{12E^3 Hg(\rho_a-\rho_w)}\right)^{1/4}$	varied
c_6	$r^2\left(\frac{12g(\rho_a-\rho_w)(1-\nu^2)}{EH^3}\right)^{1/4}$	varied
γ_1	$\frac{\rho_a}{\rho_m}$	1.27
γ_2	$\frac{(\rho_l-\rho_m)}{\rho_m}\left(\frac{12gH(\rho_a-\rho_w)(1-\nu^2)}{E}\right)^{1/4}$	0.70
γ_3	$\frac{\rho_m}{\rho_a-\rho_w}$	1.3

3. Results

3.1. Time Evolution of the Model

The governing equations are solved numerically using the pseudo-spectral method [*Canuto et al.*, 1988] with 128 × 256 Fourier modes. Figure 2 illustrates the general time evolution of the stresses during formation of intraplate volcanoes. The first pathways to the surface develop in pristine, unflexed lithosphere, resulting in the formation of a volcanic edifice (Figure 2a). Further eruptions in the vicinity of this growing volcanic load are precluded by increasingly compressive flexural stresses. The volcanic center itself, while also affected by the same flexural stresses, remains active because erosion of the fracture walls provides a positive feedback which keeps the magma pathways open.

As the lithospheric plate moves on with respect to the stationary hotspot, the plume magma source eventually encounters a region where the compressive flexural stresses are lower than the plume stress (Figure 2b) and a new eruption starts (Figure 2c), after which the process repeats itself.

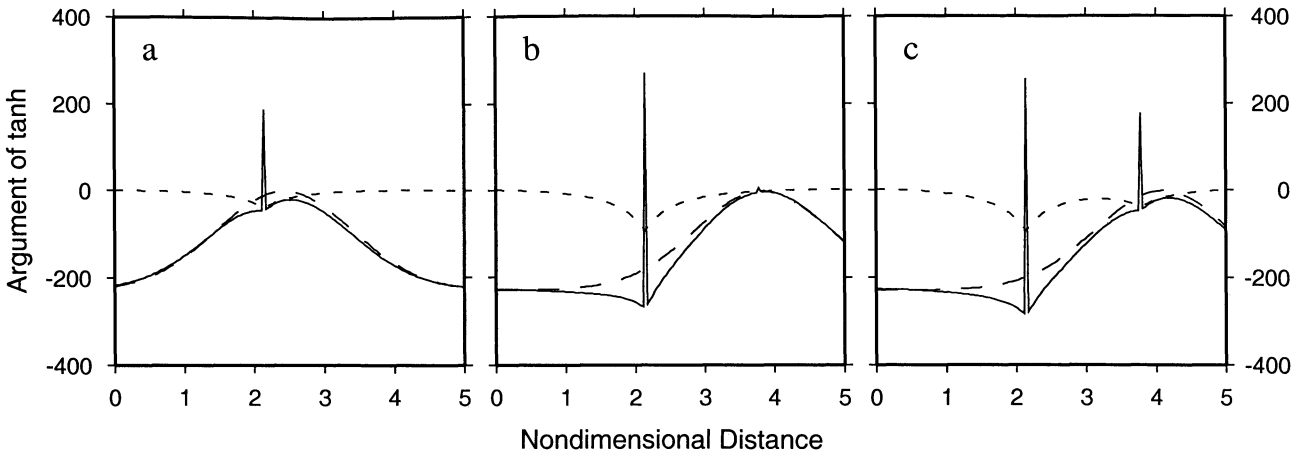

Figure 2. Evolution of stresses and erosion. The solid curve represents the entire argument of the permeability function (i.e., the argument of the tanh function in equation (7)), the long dashes are the plume stress, and the short dashes are the flexural stresses. The spikes are due to the erosional feedback. (a) The volcano (centered on the spike) is in the shield-building stage and is located near the center of the plume. Flexural stresses preclude further eruptions near the existing edifice. (b) The plume has moved to a position where the sum of the stresses is zero and a new volcano can form. The eruption is immediately focused due to fracture wall erosion. (c) The height of the volcano (which is proportional to the height of the spike) quickly increases, and the cycle repeats itself. Solidification of the dikes is neglected; hence the spikes do not decay with time and the magma flow stops when the hydraulic head balances the driving pressure.

The shape of shield volcanoes is controlled by gravity-induced spreading of the volcanic edifice [*McGovern and Solomon*, 1993, 1997; *Turcotte and Schubert*, 1982]. As the model does not take this process into account, the volcanoes generated by the model typically are narrow peaks which represent the horizontal extent of the eruptive region rather than the area covered by the volcanic edifice.

In the model, magma flux through a volcanic conduit shuts off as the magnitude of the hydraulic head approaches the driving pressure; hence all volcanoes attain the same height. Consequently, both the mass of the edifice and the resulting flexural stresses are typically greater if horizontal spreading of the volcanic edifice is taken into account. Two competing processes are involved: Horizontal spreading (while keeping the same summit height) increases the total mass of the edifice, while distribution of the mass causes the flexural curvature of the lithosphere (especially at the center of the flexure) to be less pronounced. The second effect is illustrated in Figure 3. As an example, Mauna Loa, with a total volume of 42,500 km^3 [*Bargar and Jackson*, 1974] and height of 9 km above the seafloor, may be approximated by a Gaussian of about 30 km halfwidth. As shown in Figure 3, distribution of mass to the same extent as Mauna Loa results in a decrease in flexural stresses by a factor of 2 relative to a point load of equal mass (on lithosphere of thickness $h = 30$ km). Using the same scaling, the volcanic spikes generated by our model typically have a volume of around 1000 km^3 and are thus ~40 times less massive than the distributed edifice. If the volcanoes of the model are allowed to spread out to the same extent as Mauna Loa, the increase in total mass dominates the stress change due to redistribution of mass, and the resulting flexural stresses are more than an order of magnitude greater. This consideration is important as such a model would likely require different parameter values c_3, c_4, and c_5 to produce the same qualitative results as described in the present study.

3.2. Parameter Study

The system of governing equations (10) to (12) is controlled by nine nondimensional parameters. Three of these parameters, γ_1, γ_2, and γ_3, are defined in terms of constants whose values are assumed known (i.e., g, H, D, and the

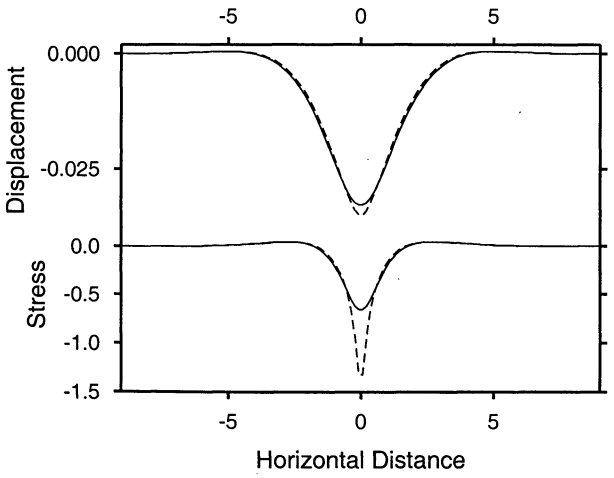

Figure 3. Flexural displacement and resulting stresses due to point load (dashed lines) and distributed Gaussian load of equal mass (solid lines). The half width of the Gaussian mass distribution with respect to the lithospheric thickness was chosen to be representative of a large volcano such as Mauna Loa.

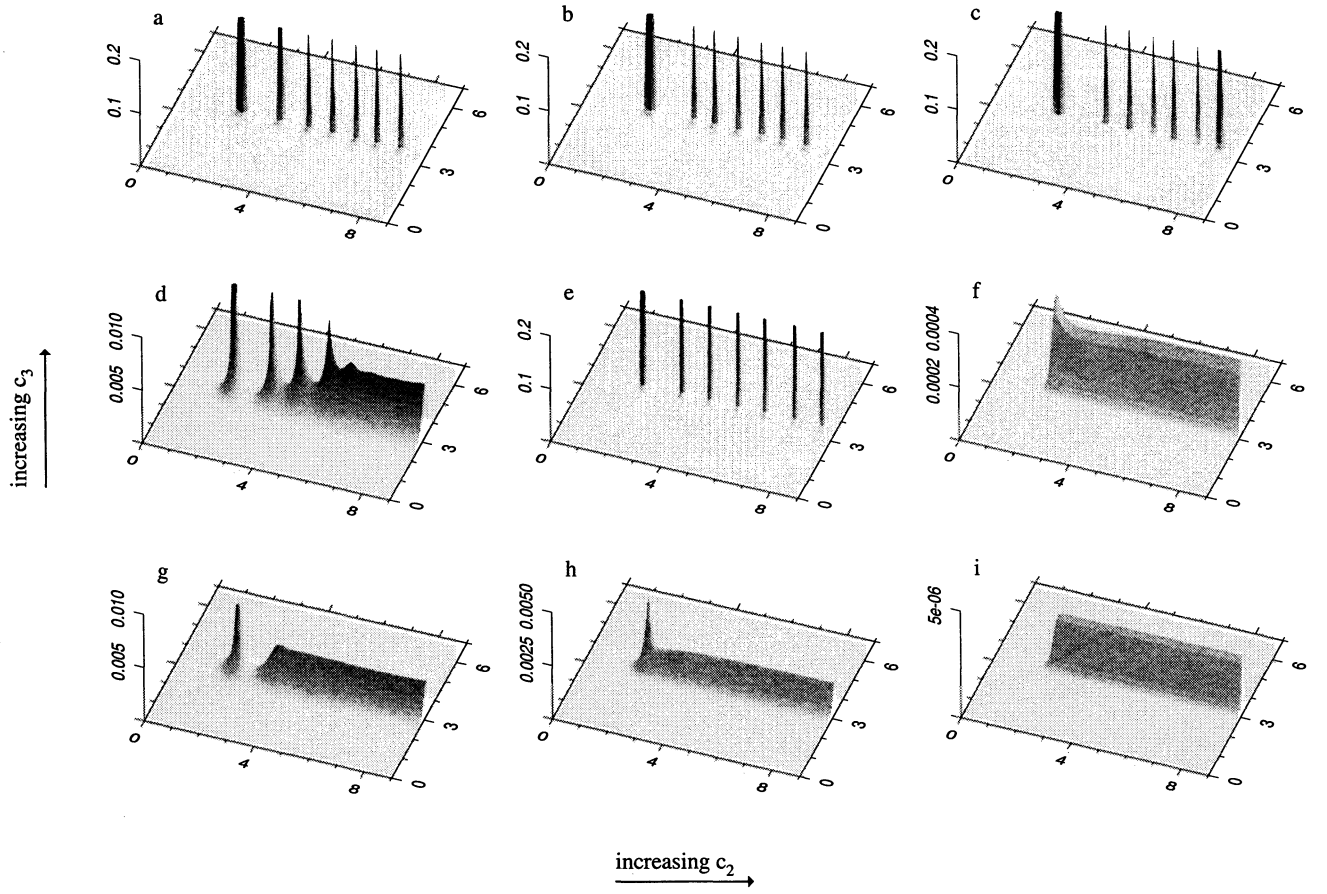

Figure 4. Model results for different values of parameters c_2 and c_3. Graphs show height of volcanic edifices as function of horizontal space. Parameter values c_2 and c_3 increase from Figure 4a to Figure 4i as indicated by arrows. The exact parameter values are summarized in Table 3.

various densities); these parameters are not varied. Four of the remaining six parameters, c_2, c_3, c_4, and c_6, are varied systematically to determine what different types of characteristic behavior of the model are possible, and how observables such as volcano spacing and volcano sizes are controlled by the parameters (parameter c_1 mostly controls the timescales over which individual volcanoes form, while changes c_5 largely reduplicate the results of varying c_3). In the following sections, the model results will be described in terms of the mathematical formulation of the model. In section 4, these results will be interpreted in terms of the physical processes.

The results shown are not necessarily representative. Instead, the most interesting results are depicted, such as the transition between continuous ridges and volcanoes. These transitions take up a very small volume of parameter space, with most of the volume occupied by ridges and volcanoes.

3.2.1. Amplitude of plume pressure. Parameter c_3 determines the effect of the plume on the permeability of the lithosphere. Figure 4 shows model results for variations in parameters c_2 and c_3; each vertical column represents changes in c_3 while holding all other parameters fixed. The parameter values are given in Table 3. The most striking observation is that the plume amplitude is a critical factor in determining the fundamental characteristics of the results; large values of c_3 generate discrete volcanoes, while smaller c_3 generally result in a continuous ridge. This behavior is easily understood in terms of the model. At low plume amplitudes c_3 the stresses alone are too small to cause any significant opening of fractures. The resulting magma flux through the lithosphere is minor, and the feedback due to melting and erosion remains insignificant because the supply of energy into the lithosphere is insufficient. However, as c_3 is increased, the amount by which fractures open above the plume center increases accordingly, causing greater permeability and magma flux. Once this flux becomes large enough, the erosional feedback mechanism is able to overpower the compressive flexural stresses caused by the growing volcanic edifice. In this regime, the effect of conduit wall erosion dominates over the flexural stresses for all values of h, and thus the volcano grows until hydrostatic balance is achieved, with the permeability now only determining the timescale of volcano formation, unable to shut off the flow. In the vicinity of the volcano the flexural stresses inhibit significant magma flow, which would allow fracture wall erosion to take place. Both magma flow due to plume stress and erosion do not become effective again until the plume is located underneath a region of low flexural stress. In this

Table 3. Values of Dimensionless Parameters

Figure	c_2	c_3	c_4	c_5	c_6
4a	5.96×10^3	2.32×10^{-3}	6.71×10^{-2}	2.56×10^{-3}	2.91
4b	8.94×10^3	2.32×10^{-3}	6.71×10^{-2}	2.56×10^{-3}	2.91
4c	2.23×10^4	2.32×10^{-3}	6.71×10^{-2}	2.56×10^{-3}	2.91
4d	5.96×10^3	2.42×10^{-3}	6.71×10^{-2}	2.56×10^{-3}	2.91
4e	8.94×10^3	2.42×10^{-3}	6.71×10^{-2}	2.56×10^{-3}	2.91
4f	2.23×10^4	2.42×10^{-3}	6.71×10^{-2}	2.56×10^{-3}	2.91
4g	5.96×10^3	2.58×10^{-3}	6.71×10^{-2}	2.56×10^{-3}	2.91
4h	8.94×10^3	2.58×10^{-3}	6.71×10^{-2}	2.56×10^{-3}	2.91
4i	2.23×10^4	2.58×10^{-3}	6.71×10^{-2}	2.56×10^{-3}	2.91
8a	8.94×10^3	2.58×10^{-3}	6.71×10^{-3}	2.56×10^{-3}	2.91
8b	8.94×10^3	2.58×10^{-3}	2.01×10^{-2}	2.56×10^{-3}	2.91
8c	8.94×10^3	2.58×10^{-3}	3.36×10^{-2}	2.56×10^{-3}	2.91
8d	8.94×10^3	2.58×10^{-3}	5.37×10^{-2}	2.56×10^{-3}	2.91
8e	8.94×10^3	2.58×10^{-3}	1.01×10^{-1}	2.56×10^{-3}	2.91
8f	8.94×10^3	2.58×10^{-3}	1.41×10^{-1}	2.56×10^{-3}	2.91
10a	8.94×10^4	2.58×10^{-3}	2.01×10^{-2}	2.56×10^{-3}	11.63
10b	8.94×10^4	2.58×10^{-3}	2.01×10^{-2}	2.56×10^{-3}	46.51
10c	8.94×10^4	2.58×10^{-3}	2.01×10^{-2}	2.56×10^{-3}	72.46
10d	5.96×10^7	2.559×10^{-3}	1.68×10^{-1}	2.558×10^{-3}	26.18
10e	5.96×10^7	2.559×10^{-3}	1.68×10^{-1}	2.558×10^{-3}	29.07
10f	5.96×10^7	2.559×10^{-3}	1.68×10^{-1}	2.558×10^{-3}	72.46
11	7.45×10^7	2.558×10^{-3}	6.71×10^{-2}	2.558×10^{-3}	2.91
12	8.94×10^4	2.54×10^{-3}	6.71×10^{-2}	2.588×10^{-3}	24.57

light, it is also clear that it really is the difference between the plume stress amplitude, given by c_3, which determines the characteristics of the results, provided c_5 is large enough to prevent eruptions away from the hotspot. Variations of c_5 are therefore not investigated independently.

With further increases in c_3, the fundamental character of the solution does not change (Figure 4c), unless the plume stress is increased so much that flexural stresses become negligible and all effects of the lithosphere are removed (results not shown). The model continues generating discrete volcanoes, but the intervolcanic spacing decreases because the greater plume stress is able to overcome the compressive flexural stresses closer to previously formed edifices (Figure 5).

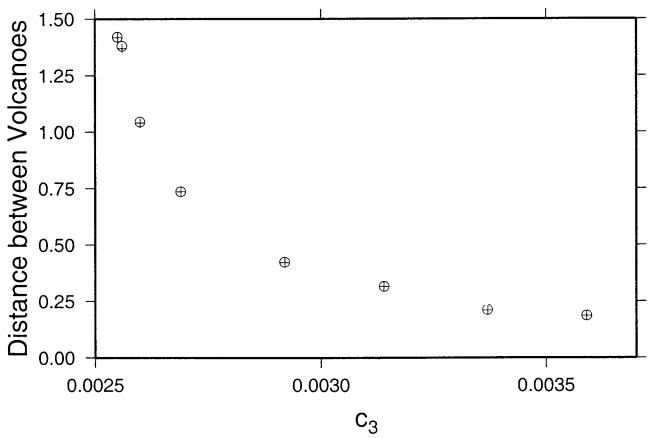

Figure 5. Volcano spacing as a function of plume stress (parameter c_3). Circles denote results for $c_4 = 0.0671$, crosses denote results for $c_4 = 0.0336$. Values reported for intervolcanic distances are average of about 10 spacings after the transient behavior has decayed away.

The first volcano is larger in horizontal extent because during its formation there is no interaction with the flexure of any older volcanoes; if the amplitude of c_3 of the hotspot pressure is great enough, a relatively large area surrounding the center of the hotspot is subject to eruption. For subsequent volcanoes, eruptions are precluded until the leading edge of the plume has reached a region where the sum of the stresses is barely great enough to allow volcano formation. This first eruption impedes further eruptions in the vicinity due to the quickly growing flexural stresses.

The spacing is always greater following a large volcano, especially the initial one. To the extent that all volcanoes can be approximated as point loads, the distance from the center to the zero-crossing of the flexural displacement is the same for volcanoes of different amplitude, as is the distance to the location of zero net flexural stress ($\sigma_f = 0$), while the amplitude of the flexural displacement depends linearly on the mass of the edifice. If the model parameters are chosen such that a volcano can barely form in a location of zero flexural stress, then the spacing will be the same between volcanoes of different mass. This important special case is examined in section 3.6. In Figures 4g and 4h, the plume stress is greater than the background stress, and hence the second and all subsequent volcanoes form inside the zero-flexural stress radius of the previous volcanic edifice, i.e., where the flexural stress is compressive. For small volcanic loads the location is relatively close to the center of the load, whereas for large loads this position approaches the position

of $\sigma_f = 0$. In the present model, larger spacing is thus expected following greater volcanic loads. As the plume stress is increased to (unrealistically) large values, the spacing goes to zero: a continuous ridge is formed in this way when the magma pressure overcomes the compressive flexural stresses near the center of the nearest volcanic edifice, which in the case of Hawaii are of the order of a few hundred megapascals.

3.2.2. Slope of the permeability function. Parameter c_2 multiplies the argument of the permeability function and thus $(c_2)^{-1}$ determines the domain over which the stresses and the melting and erosional effects cause significant changes in permeability. Equivalently, c_2 determines the maximum slope of the permeability curve versus stresses and melting; that is, a large c_2 causes an abrupt transition from low to high permeability. Figure 4 shows solutions for which the value of c_2 is varied for three different values of c_3.

As demonstrated by the second row of results (Figures 4d-4f), parameter c_2, like parameter c_3, partially determines whether the model output consists of discrete volcanoes or of a continuous ridge. For the case of intermediate plume stress $c_3 = 2.42 \times 10^{-3}$ and for increasing c_2, the model makes a transition from a continuous ridge to discrete volcanoes around $c_2 = 5.96 \times 10^3$ and back to a continuous ridge around $c_2 = 1.95 \times 10^4$. One such case near the threshold value of c_2 is shown in Figure 4d, but the transition between the two dominant modes of model output generally follows a similar pattern: with increasing c_2, the initial pulse of magma increases in amplitude as the hotspot is "switched on." If c_2 is just below the threshold, the subsequently formed ridge displays some undulations which decay over time. Over a very narrow range of increasing c_2, these undulations increase in amplitude and decay more slowly over time. Beyond the transition, the undulations are stable in time and an infinitely long line of volcanoes is formed.

For the case of varying c_2, there are two processes which cause the transitions between the continuous ridge and discrete volcanoes as shown in Figures 4d–4f. At low values of c_2 a wide area of lithosphere around the plume is in a range where the permeability is nonzero, thus causing broader edifices. Even though the height of the volcano is low, its width and thus its total mass nonetheless cause significant flexural stresses. For small c_2 the erosional feedback effect is therefore always dominated by the flexural stresses. The model thus restricts itself to remain in a nearly linear state, and a continuous ridge ensues. As c_2 is increased, the permeability of the lithosphere over the plume center increases much more than in the surrounding area. This is because with a high value of c_2 (i.e., a low value of C_o, see Table 2), small changes in porosity f cause a larger change in C (5). In addition, (4), with C given by (5), describes a nonlinear relation between $d\sigma_p$ and df, whose integral form is given by the hyperbolic tangent of the permeability relation (6). A small σ_p variation is thus amplified nonlinearly into a much greater variation in porosity and permeability. While the increase in c_2 causes a general increase in the amplitude of permeability, the permeability also becomes much more concentrated toward the plume axis, and the more focused magma flux implies that the flexural stresses are no longer sufficient to overwhelm the erosional feedback. Volcanoes can then grow to the maximum height allowed by the hydrostatic pressure, resulting in a line of discrete volcanoes. In Figures 4a–4c, this transition is not shown, but for sufficiently low values of c_2 the model does generate a continuous ridge.

As c_2 is increased further, a second transition, from dis-

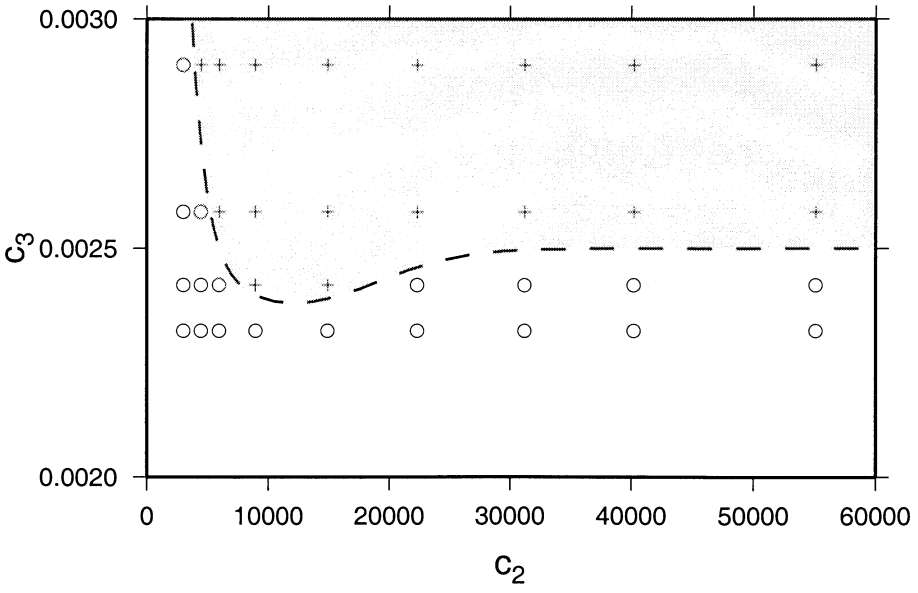

Figure 6. Model results for different values of parameters c_2 and c_3. Results of discrete volcanoes are indicated by crosses, and continuous ridges are indicated by circles. Approximate region of discrete volcano formation is shown as shaded area. Other parameters are the same as for Figure 4 (see also Table 3).

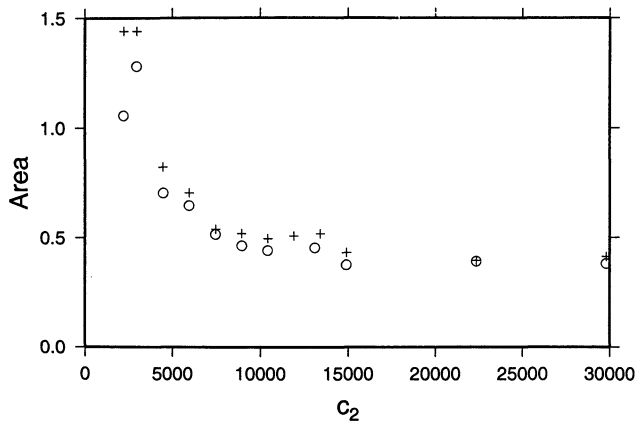

Figure 7. Size of eruptive region as a function of parameter c_2. Increasing values of c_2 result in increased focusing of eruptions.

crete volcanoes back to a low-amplitude continuous ridge (Figure 4f), occurs if the peak of the plume stress is lower than the impeding background stress c_5. For large c_2 the transition from near zero to nonzero permeability becomes sharper and thus the peak plume stress no longer puts the permeability into the nonzero domain. The effect is thus similar to changing c_3, but instead of lowering the plume pressure, here the permeability function is such that the plume stress cannot induce significant permeability. In Figures 4g–4i the plume stress is too low and a continuous ridge forms for all values of c_2. In Figures 4a– 4c the plume stress is higher than the compressive background stress and discrete volcanoes result. Figure 6 illustrates the parameter space defined by parameters c_2 and c_3 and shows the regime in which discrete volcanoes form.

Parameter c_2 also has more detailed effects both on the continuous ridge and the discrete volcanoes. The height of the continuous ridge (for the given parameter values) decreases with increasing c_2 (Figures 4g– 4i) because the plume stress is less able to induce nonzero permeability. Perhaps more importantly, in the case of discrete volcanoes the horizontal extent of the eruptive area diminishes as c_2 is increased (Figures 4a–4c and 7). The focusing of the magma into a narrow conduit becomes more pronounced and appears to be limited only by the resolution of the numerical grid.

3.2.3. Strength of melting and erosion. As already mentioned in section 2, the combined effects of melting and erosion of the fracture walls result in a nonlinearity, which provides a positive feedback on the magma flow. Figure 8 illustrates the model results for varying parameter c_4 which controls the magnitude of this feedback. Like parameters c_2 and c_3, parameter c_4 also partly determines whether the model generates discrete volcanoes or a continuous ridge. We determined, from a large number of model runs (only some of which are shown in this paper) that for a wide range of c_2 and c_3 the model yields discrete volcanoes for sufficiently large c_4. However, the converse is not true; that is, for low values of c_4, there are no parameter combinations which will result in discrete volcanoes (Figure 9). The effect of melting and erosion which is quantified by parameter c_4 is thus the dominant process which determines which of the two possible model outputs results. The significance of parameter c_4 is to be anticipated from the physics included in the model; while the flexural stresses provide a mechanism that keeps the lithosphere impermeable around an existing volcanic edifice, a separate process, namely, erosion of the fracture walls, is required to keep a conduit open directly underneath the volcano.

Figure 8 also shows that parameter c_4 has some control over the shape and size of volcanic edifices. For the case of the continuous ridge (Figures 8a–8c), larger values of c_4

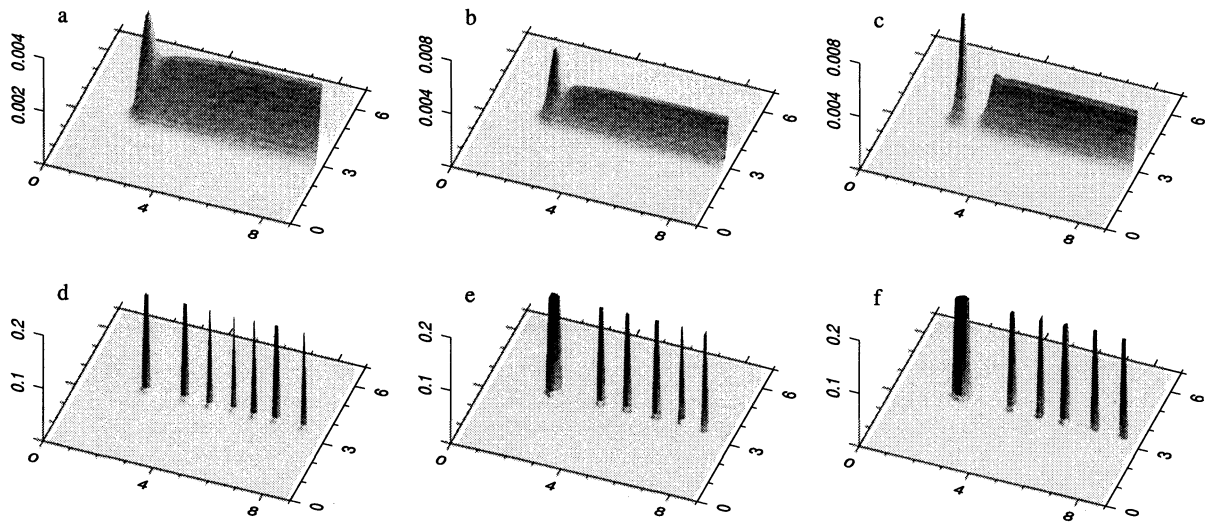

Figure 8. Model results for different values of parameter c_4. All other parameters are held constant. The value of c_4 increases from Figure 4a to Figure 4f as shown in Table 3.

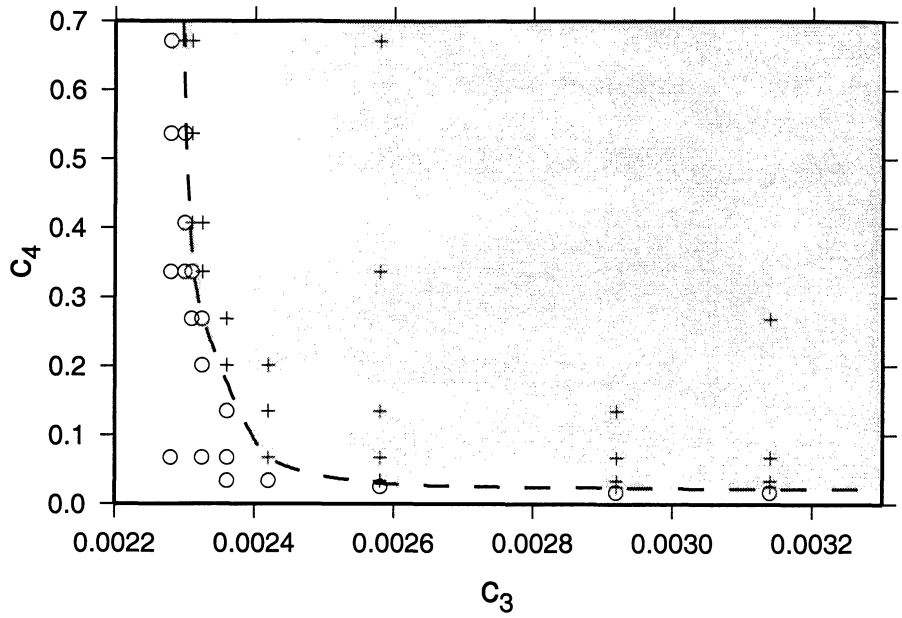

Figure 9. Model results for different values of parameters c_3 and c_4. Results of discrete volcanoes are indicated by crosses, and continuous ridges are indicated by circles. Approximate region of discrete volcano formation is shown as shaded area. Other parameters are $c_2 = 1.49 \times 10^4$ and c_5 and c_6 as in Figure 4.

result in a ridge of larger amplitude. While the effect of melting and erosion is less than that of the compressive flexural stresses, the minor magma flux which forms the ridge is nonetheless aided by an increase in permeability due to melting and erosion. As the value of c_4 is increased further and discrete volcanoes form, the size of the eruptive area is slightly enlarged for increasing values of c_4.

As the eruptive area of the volcanoes grows larger (Figures 8e and 8f), the shape of this area becomes more elongate in the direction perpendicular to the trend of the volcanic line. This happens because the position of the new eruption is mostly controlled by the flexural stress of the previously formed volcano (which has already grown to significant size). In the region of interest the stress field is approximately that due to an isolated point load (i.e., the rest of the line of volcanoes only has a minor effect), and thus the new volcano is constrained to form on or beyond a circular arc on which the flexural stresses are sufficiently low. The most favorable position for volcano formation is, of course, on the hotspot axis, but for the given parameter values, locations slightly off axis are affected only slightly less by the pressure of the approaching plume, and eruptions start along an elongate, axis-centered part of the circular arc dictated by the flexural stresses. This tendency is accentuated by plume stress functions which are less peaked, either due to a wider Gaussian function, or a more plateau-shaped super-Gaussian function with parameter $p > 1$ (see section 3.2.4 on varying c_6).

3.2.4. Width of high plume stress region. The width of the Gaussian plume stress function is determined by parameter c_6. Figure 10 shows two sets of model results, each with constant parameters c_2 to c_5, while parameter c_6 is varied. Figures 10b and 10c show two different cases of continuous ridges. For lower values of c_6 (i.e. a more peaked Gaussian function), the ridge is both narrower and higher. The variation in width of the ridge is intuitive since the ridge mostly reflects the shape of the Gaussian plume stress modulated by the strongly variable permeability function (10). However, there is some additional modification in shape due to the two feedback effects. The positive feedback due to melting and erosion affects both ridges equally (to first order), but the negative feedback due to compressive flexural stresses is larger for the wider and thus heavier ridge. Thus the narrower ridge can build to a greater height.

In Figure 10a the same model with lower c_6 results in a line of discrete volcanoes. The reason for this transition is the same as for the different amplitudes of the ridge in Figures 10b and 10c; for an even narrower plume stress the compressive flexural stresses inhibiting flow are lower and in this case no longer dominate over the effects of melting and erosion.

Figures 10d–10f show similar model outputs for different values of c_2 through c_5 in order to investigate the effect of c_6 on discrete volcanoes. For a narrow Gaussian plume stress (small c_6) the model results in a single line of volcanoes. For increasing values of c_6, off-axis volcanism occurs. At intermediate values of c_6, two symmetrically located off-axis volcanoes form following the initial larger volcano, while subsequently the model reverts to producing a single line. Increasing c_6 further makes the plume stress wide enough to allow volcano formation in a region of radius greater than the volcano spacing (Figure 10f), and a symmetric pattern of volcanoes ensues which is ~3 to 4 volcano spacings wide.

The set of parameters used to generate Figures 10d–10f had to be chosen fairly carefully to allow such results; with parameter $p > 1$ the plume stress is transformed from Gaus-

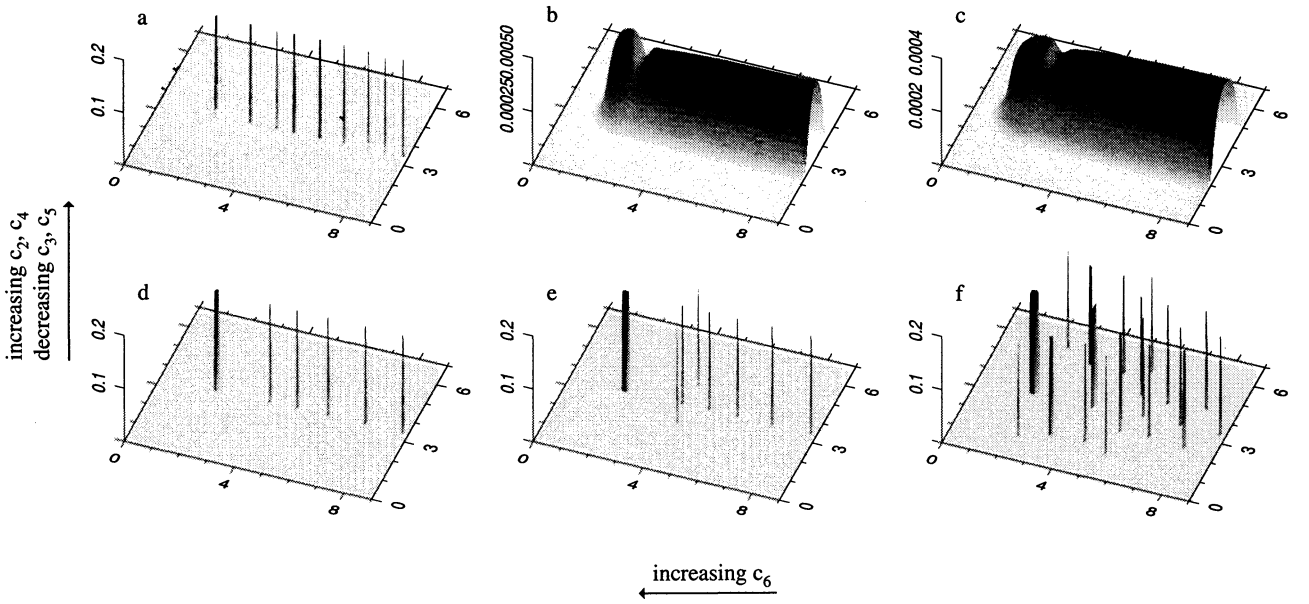

Figure 10. Model results for different values of parameter c_6. Between Figures 10a–10c and Figures 10d–10f, parameters c_2, c_3, c_4, and c_5 were all changed in order to sample the small region of parameter space in which more complex patterns of volcanoes (such as Figure 10f) are possible. With a super-Gaussian plume stress (i.e., $p > 1$), similar patterns occur over a wider range of parameters. If the plume stress is interpreted as being mostly due to low viscosity of melt when compared with the surrounding asthenospheric material (i.e., viscous head loss of the asthenosphere with respect to the plume), then the parameter values (including p) are likely such that complex volcano patterns occur. (See text for details. See also Table 3 for a summary of parameter values used.)

sian to a more plateau-shaped super-Gaussian (approaching the boxcar function), and wide patterns of discrete volcanoes follow much more naturally.

3.2.5. Equidistant spacing. To a large extent, the inter-volcanic spacing can be explained in terms of the amplitude of the plume stresses and their interactions with the flexural stresses (see section 3.2). However, it was generally observed that the gap following the first, large volcano is greater than the subsequent spacing between smaller volcanoes. Given the results obtained so far, an intelligent guess may be attempted at parameters necessary to generate equal spacing between volcanoes of all sizes.

It is expected that $c_3 = c_5$ and $c_2 \to \infty$ is such a parameter combination. With $c_2 \to \infty$, the permeability approaches a step function. Eruptions thus first occur at a point where the permeability changes abruptly from zero to nonzero, which occurs where the stresses add up to zero. Letting $c_3 = c_5$ sets the maximum value of the plume stress to zero, so that eruptions start at the position where $\sigma_f = 0$, which is in the same location with respect to the center for volcanoes of any mass.

The results of this experiment are shown in Figure 11, generated using the same parameters. The only difference between Figures 11a and 11b is the initial condition; in Figure 11a the model is initialized by manually placing a fairly large volcano on the hotspot axis on top of the initial location of the hotspot. In Figure 11b a much smaller volcano is placed in the same location. It is clearly seen that our efforts were not very successful; that is, the volcanoes in Figure 11 are generally not equally spaced.

However, in both cases the second volcano did form in exactly the same location, even though the first volcano in 11a is 9 times larger than the first volcano in 11b, and the flexural stresses of those two volcanoes differ by the same factor. The reason the model does not produce equidistant spacing for all volcanoes is that new volcano formation depends on the flexure due to the most recent volcano and its predecessor since both older volcanoes determine the position of zero flexural stress and hence the location of the new volcano. For volcanoes of equal size the stresses of the flexural bulge due to the older volcano are always the same and are small with respect to the flexural stresses of the nearest volcanic edifice. However, when the more distant volcanic load is several times larger than the closest one, the effect of its flexural bulge becomes significant. It therefore appears that the model is unable to generate equal spacing for volcanoes of different mass. This interesting result is in contrast to the assumption that the locations of volcanoes are determined only by the flexural stresses due to the most recent volcanic load [*ten Brink*, 1991] but are also influenced by mass of preceding loads, as well as other processes (magma flow, magma source width, etc.).

3.2.6. Initial off-axis perturbations. It was shown in Figure 10f that a sufficiently wide plume stress region results in a wide pattern of volcanoes instead of a single line. The symmetry of the single-line pattern may also be broken by an

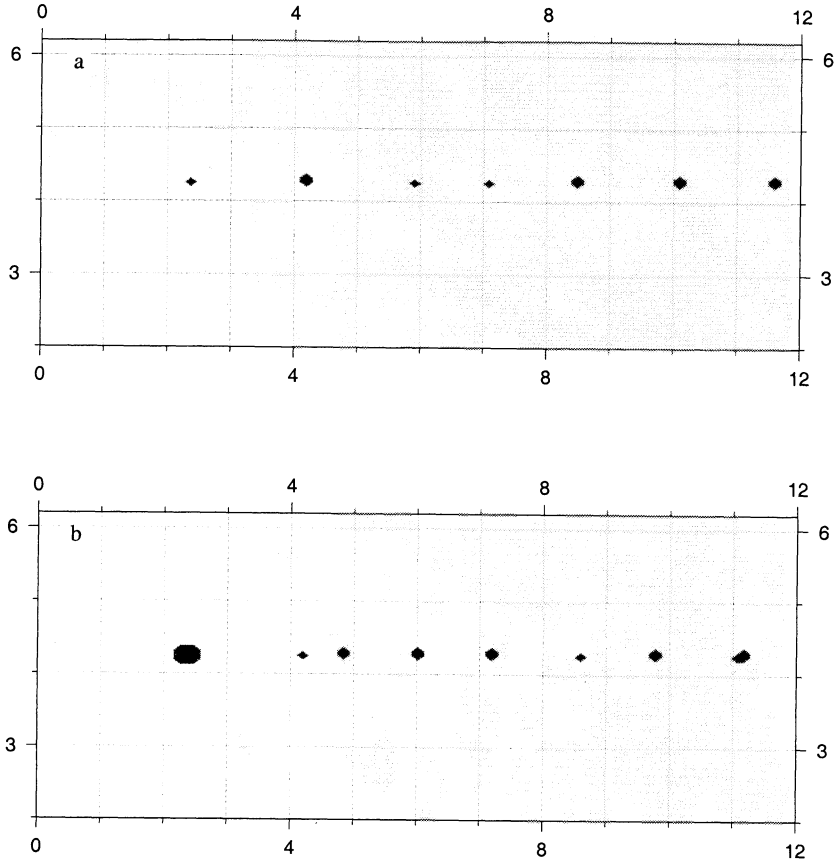

Figure 11. Map view of volcano locations. (a) Evolution following a small initial volcano. (b) Evolution following a large initial volcano. Comparison of Figures 11a and 11b shows that when $c_2 \to \infty$ and $c_3 = c_5$, the distance from an initial (isolated) volcano to the next volcano is the same regardless of the size of the first edifice. However, subsequent volcanoes are affected by the flexure of the prior two to three volcanoes, resulting in different spacing after the second volcano. (See text for details. See also Table 3 for parameter values used.)

initial off-axis load. Such a perturbation also allows for the formation of a dual line of volcanoes. With $p \geq 3$ the plume stress assumes a pronounced plateau shape; dual lines and other wide patterns of volcanoes then occur for a wide range of parameters (c_2 has to be large in order to produce nearly point-like volcanoes; with small c_2 the volcanoes become increasingly crescent-shaped).

An initial load placed slightly off axis causes a perturbation in the results which grows over time (Figure 12a). Eventually, a stable pattern is reached in which any three adjacent volcanoes approximately form an equilateral triangle. The volcanoes are thus positioned in an alternating double line. The separation between the lines is ~0.87 times the intervolcanic spacing. With a greater initial perturbation this stable state is reached more quickly (Figure 12b). A further increase in the initial perturbation does not change the results qualitatively (Figure 12c). Figure 13 illustrates the growth of a small initial perturbation over time.

If the plateau of the plume stress σ_p is wider than the maximum separation between two lines, the dual line tends to meander (Figures 12b and 12c). Further experiments (not shown) were unable to change significantly the curvature of this meander (for example, by changing p which parameterizes the shape of the plume stress).

For the continuous ridge, initial off-axis perturbations only change the transient behavior before the same steady state as that for the unperturbed ridge is reached (result not shown).

4. Discussion

In section 3 it was seen that all of the parameters interact to determine the characteristic output mode of the model (i.e., discrete volcanoes or continuous ridge), the spacing and width of the volcanoes, the height and width of the ridge, and the width of the pattern of volcanoes if the volcanoes are not located in a single straight line. Nonetheless, it was observed that each parameter predominantly controls one of these features. Thus, parameter c_2 (see (10)) to a large extent controls the focusing of the magma and thus the size of the eruptive region; c_3 (together with c_5; see (10) and (12)) influences the spacing between volcanoes; c_4 determines whether the model results in discrete volcanoes or a continuous ridge; and c_6 controls the width of the swath over which volcanoes can form.

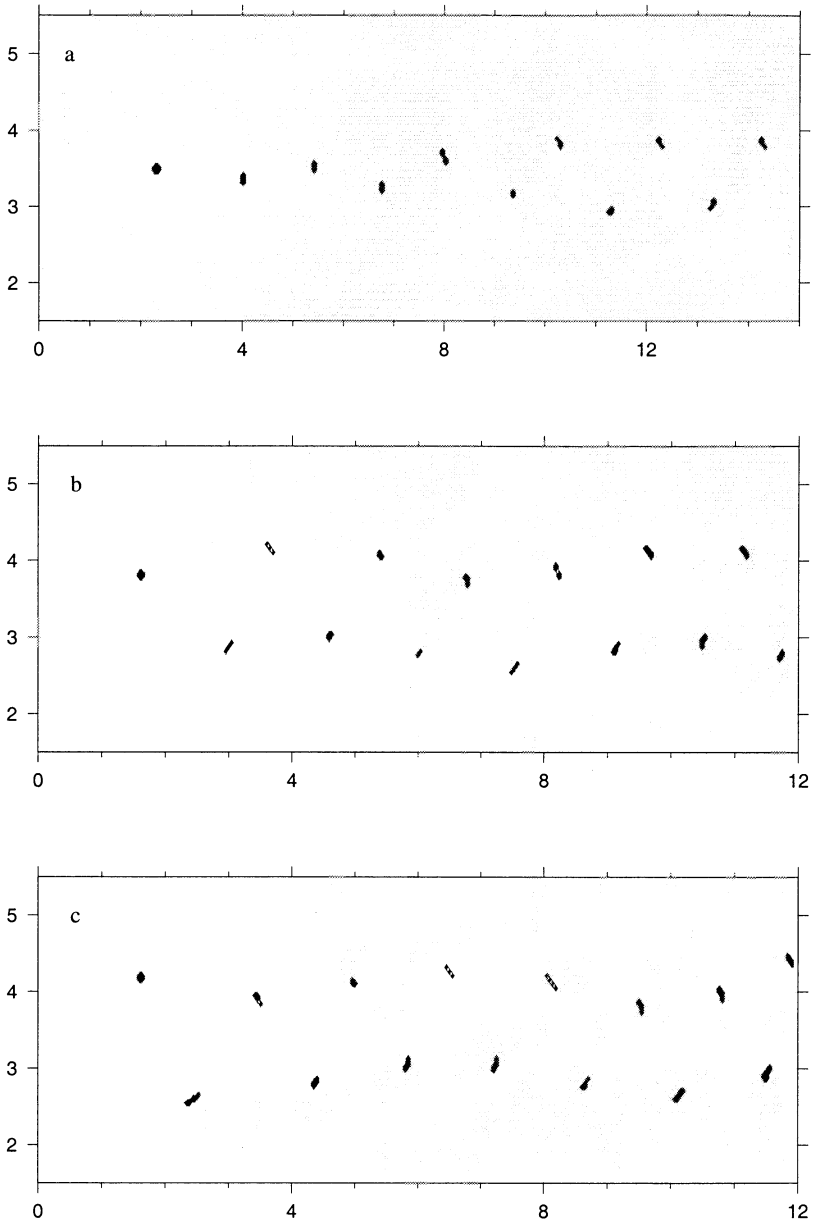

Figure 12. Map view of volcano locations for $p = 3$. (a) Small off-axis perturbations grow over time, resulting in the stable arrangement in which any three nearest-neighbor volcanoes form approximately an equilateral triangle. (b and c) For larger perturbations, the stable configuration is reached more quickly. For sufficiently wide plume stress the dual line of volcanoes meanders (Figures 12b and 12c). For wider plume stresses, triple lines and other patterns are possible (not shown).

4.1. Volcano Spacing

In the present model, as well as in the model of *ten Brink* [1991], magma flow through the lithosphere occurs via hydraulic fracturing by the magma. In the *ten Brink* [1991] elastostatic approach, a new eruption commences in a location where the magma pressure exceeds the flexural stresses, which he assumes occurs at the position of zero flexural stress. The melt pressure of the plume is thus implicitly set to a value slightly above lithostatic. The model of this study is more general and contains the *ten Brink* [1991] model as a subset; this special case was shown section 3.2.5. With a steep hyperbolic tangent function in the permeability law (large c_2), and a magma pressure that is barely able to overcome the negative background stresses ($c_3 \approx c_5$), a second volcano following an isolated first volcanic edifice was seen to form at exactly the spacing predicted by *ten Brink* [1991].

However, a first difference from the *ten Brink* [1991] model was demonstrated by including the flexural effects of the older portions of the volcanic line. When older volcanoes are massive, their flexural effects may be significant in comparison with the flexural stresses of the most recent volcano. Changes in volcano size were thus seen to result in irregular spacing, while for the same parameter values, lines consisting exclusively of large volcanoes or of small volcanoes exhibit regular spacing.

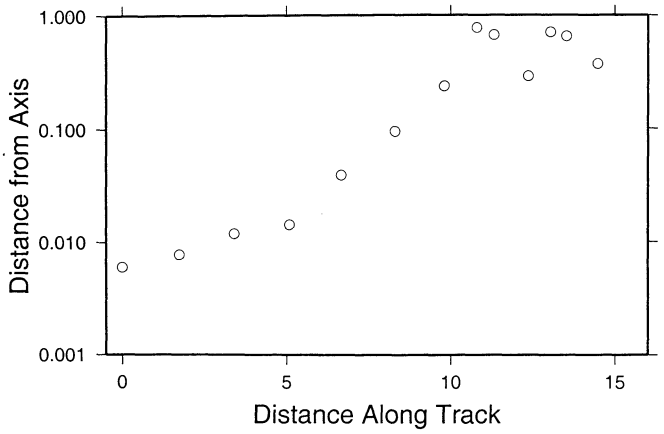

Figure 13. Growth of small initial off-axis perturbation over time.

Second, the two models differ because the present model allows for a relaxation of the *ten Brink* [1991] assumption of low plume pressure and stresses. If the plume pressure and stress are too low, no volcanoes form at all; the low continuous ridges predicted by the model may be interpreted as low volume eruptions without any characteristic spacing. For larger values of magma pressure, discrete volcanoes form with decreasing spacing for increasing plume pressure. If the value of c_2 remains large (i.e., changes in permeability are abrupt), eruptions still occur at the location where the stresses add to zero, but this position is now a function of volcano size. If c_2 is decreased, volcanoes can form even where the total stresses are compressive. In the present dynamical formulation of the model *ten Brink*'s [1991] simple relation between spacing λ and flexural rigidity D, ($\lambda \sim D^{1/4}$) is thus replaced by a more complex (and unknown) relation depending on all of the parameters specified in the model.

A third difference between the present model and the *ten Brink* [1991] model stems from the definition of the location of zero flexural stress. For an isolated point load the flexural deflection of the lithosphere is given by Hertz's solution [*Nadai*, 1963], from which analytical solutions for the radial stress σ_{rr} and the tangential stress $\sigma_{\theta\theta}$ may be derived. In the present model the stress governing the porosity due to fractures is given in analogy with the Biot theory [*Biot*, 1941] as the sum of the normal stresses, i.e., $\sigma_{rr} + \sigma_{\theta\theta}$, which is the first invariant of the horizontal stress tensor. This type of formulation is assumed to be appropriate for an isotropic medium, which for a fractured medium must be interpreted as randomly oriented fractures. The *ten Brink* [1991] model is instead defined in terms of the radial flexural stress only, i.e., volcanoes form where $\sigma_{rr} = 0$. This definition is probably more appropriate for the case under consideration, since simple fracture mechanics predicts that fractures will form as soon as the fluid pressure exceeds the least compressive stress, and the rock thus becomes anisotropically fractured (with fractures extending in the θ direction). The difference between the two models manifests itself in the distance from a volcanic load to the point of zero flexural stress. The radius from a point load to the location of $\sigma_{rr} = 0$ is $\sim 1.06\alpha$, where α is the flexural parameter defined as $\alpha = [4D/g(\rho_a - \rho_w)]^{1/4}$ (and with Poisson's ratio $\nu = 0.25$, as *ten Brink* [1991] appears to have used in his calculation; the distance varies from 0.81α to 1.30α for values of ν between 0 and 0.5). Our model instead yields a larger distance of approximately 1.72α between the load and the position of zero flexural stress, regardless of the value of ν.

4.2. Focusing of Melt

The focusing of magma from a distributed source at the base of the lithosphere into a narrow zone containing one or several fractures or conduits is largely controlled by parameter c_2 (again, see (10) and (12)). The focusing mechanism represented by large values of c_2 is simply that the first fractures forming due to slight magma overpressurization grow large in cross section almost instantaneously, and thus the new volcanic edifice rapidly increases in mass causing compressive flexural stresses in its vicinity.

Aside from a dependence on thickness and elastic parameters of the lithosphere and various densities (all of which are assumed to be known at a given location), parameter c_2 is a function the value of $\beta = 4C_o/f_{\max}$. The model was seen to produce very concentrated high-permeability regions for large values of c_2 or low ratios of β. The physical meaning of β is more easily recognized when the porosity relation in terms of stresses alone is expressed in a Taylor expansion. Neglecting the effects of melting and denoting the combination of all stresses by σ, the porosity law, where $f = k/k_o$ in (6) linearizes around the point $\sigma = 0$ to

$$\Delta f \approx \frac{f_{\max}}{\beta}\Delta\sigma. \tag{13}$$

Parameter $\beta/f_{\max}$ is thus the proportionality constant relating the stresses to the porosity. This proportionality constant is independent of the elastic moduli of the solid rock comprising the lithosphere [*Biot*, 1941]; however, β can be related to the bulk modulus of the porous rock matrix [*Guéguen and Palciauskas*, 1994]. For pores of ellipsoidal cross section the effective bulk modulus of the porous rock skeleton is

$$K_{\text{eff}} = K\left(1 - \gamma\frac{f}{A}\right), \tag{14}$$

where K is the bulk modulus of the solid rock, γ is a parameter which, for low values of f/A, is < 3.3, and A is the aspect ratio which is equal to thickness divided by width of the fractures (where length is greater than width and width is greater than thickness) [*Henyey and Pomphrey*, 1982]. The dependence of porosity on fluid pressure may be derived from first principles [*Guéguen and Palciauskas*, 1994] and in the case of no isotropic strain ($\varepsilon_{kk} = 0$) and for the fluid bulk modulus equal to the bulk modulus of the solid rock ($K_f = K$) becomes, with (14),

$$\Delta f = \frac{f}{K}\left(\frac{\gamma}{A} - 1\right)\Delta P. \tag{15}$$

Inspection of (13) and (15) and equating pore pressure $\Delta P = \Delta\sigma$ and $f = \frac{1}{2}f_{\max}$ shows that

$$\beta = 2K\left(\frac{\gamma}{A} - 1\right)^{-1}. \tag{16}$$

As might have been anticipated, the value of β which determines the elastic widening of fluid filled voids due to increases in pore pressure is generally of the order of the bulk modulus of the solid rock which has to be displaced. However, in the case of elongate, low-aspect ratio fractures the value of β is reduced by a factor equal to the aspect ratio A, which may be as low as 10^{-2} to 10^{-3}.

Using $c_2 = 8.94 \times 10^3$, which was used to generate Figure (4e), the value of β is found for typical densities and elastic coefficients ($E = 7 \times 10^{10}$ Pa, $\nu = 0.25$, $\rho_a = 3300$ kg m^{-3}) and lithospheric elastic thickness of 35 km to be $\beta = 3 \times 10^6$ Pa, which suggests a reasonable aspect ratio of the fractures of $A = 10^{-3}$. Using the same values to redimensionalize the lengths in Figure 4e, the eruptive area is seen to have a diameter of around 10 km. Further focusing is not likely by the processes parameterized by c_2, but other processes such as the interaction of upward propagating dikes [*Ito et al.*, 1997; *Muller*, 1999] or a drop in magma pressure around the source region of the active conduit may be very effective on this smaller scale. From observations the areal extent of the active or porous volume is of the order of 10 km^2 [*Ryan*, 1988].

The model prediction that the existence and size of fractures depend strongly on the stresses and on erosion of the fracture walls needs to be tested with more detailed studies using fracture mechanics coupled with melting and thermomechanical erosion. In addition, a better understanding of melt transport in the transition zone from viscous mantle to elastic, brittle lithosphere is required.

4.3. Amount of Melting and Erosion

The effects of melting and erosion of the fracture walls are clearly important for the generation of discrete volcanoes in the model. While there is some evidence of crustal and lithospheric contamination of the erupted lavas [*Eiler et al.*, 1996], general consensus is that such contamination is small [*Hauri et al.*, 1996]. It therefore remains to be verified that volumetrically minor amounts of melting and erosion may have a significant effect in the model in counterbalancing the compressive flexural stresses. This section provides some estimates of the expected porosity changes from melting alone, thus neglecting other sources of erosion.

The amount of heat lost in the magma on its traverse through the lithosphere may be calculated from estimates of the flow geometry and heat conduction. Assuming laminar flow of magma through sufficiently large fractures, the thermal boundary layer thickness Δx is of the order of 20 cm, using $\Delta x = (\kappa H/v_m)^{1/2}$, where $\kappa = 10^{-6}$ m^{2}s^{-1} is the thermal diffusivity, $H = 35$ km, and $v_m = 1$ m s^{-1} is the average magma velocity [see *Bruce and Huppert*, 1990]. The average temperature drop in the magma is of the order of $\Delta T = (T_{\text{magma}} - T_{\text{wall}})\Delta x/w$, where w is the thickness of the fracture. Assuming $w \approx 1$–10 m [*Lister and Kerr*, 1991] and $(T_{\text{magma}} - T_{\text{wall}}) \approx 100°$C [*Rubin*, 1995], the temperature drop is about $\Delta T \approx 2 - 20°$C. The heat loss in the magma is thus found to be of the order of $\Delta Q = \rho_m c_p \Delta T \approx 1 \times 10^7$ J m^{-3}, using a value of heat capacity of $c_p = 7 \times 10^2$ J kg^{-1} K^{-1}) [*Bruce and Huppert*, 1990].

If all the heat lost from the magma goes into melting of wall rock, then the differential change in porosity during a small increment in volcano height is

$$\frac{df}{dh} = \frac{\Delta Q}{H\rho_m L}, \tag{17}$$

where L is the latent heat of melting of the wall rock. The right-hand side of (17) does not contain a factor of f; while the amount of magma within the porous rock matrix and thus the heat transferred from it clearly scale by a factor of f, once the magma reaches the surface it spreads out again to form a volcanic edifice of height h whose basal area is assumed to be the same area over which we defined the porosity (i.e., porosity is defined as cross-sectional area of pores divided by the basal area of the volcano). An equivalent relation is given in the model by (4) keeping the stresses fixed. The efficiency of melting is greatest at $f = \frac{1}{2}f_{\max}$, which is thus the proper point for comparison:

$$\frac{df}{dh} = \frac{f_{\max}^2}{4HC_o} B\Delta Q. \tag{18}$$

Comparison of (17) and (18) yields the desired relation for B:

$$B = \frac{4C_o}{\rho_m L f_{\max}^2}. \tag{19}$$

This value may in principle be compared with the value of B used for the model calculations; however, since the value of $f_{\max}$ has never been determined, (19) really just gives us an equation for the maximum porosity. Using $B\Delta Q = 1.3 \times 10^{10}$ Pa (the value used to generate most of the figures), $4C_o/f_{\max} = 3 \times 10^6$ Pa, $L = 8 \times 10^5$ J kg^{-1} [*Bruce and Huppert*, 1990], and the calculated value of $\Delta Q = 1 \times 10^7$ J m^{-1}, we can solve for the only unknown in (19), i.e., $f_{\max} = 5 \times 10^{-6}$. This value of $f_{\max}$ is the upper bound on porosity that the model predicts, assuming that all porosity is caused by melting. If the assumed porosity on the kilometer scale of the model is greater, then the heat transferred from the magma into the wall rock is not sufficient to effect the required magnitude of melting. As indicated in section 2, two alternative interpretations are possible, depending on whether the maximum porosity $f_{\max}$ is assumed to be a material property of the lithosphere or the result of more complex dynamical interactions. If $f_{\max}$ is the disaggregation limit of the porous matrix, which is typically of the order of $0.01 \leq f_{\max} \leq 0.1$, then the energy available for melting of the fracture walls is not sufficient to cause the required porosity change, and other energy inputs such as gravitational potential or chemical energy are necessary. On the other hand, if $f_{\max}$ is the result of short-term interactions between melt supply and elastic stresses, much lower values

of f_{max} are possible. Estimating the total cross-sectional area of the magma conduits of a given volcano ($\sim$1 m^2 for laminar flow in a single, cylindrical conduit, with $\mu = 100$ Pa s [*Bruce and Huppert*, 1990], $Q = 3.6$ m^3 s^{-1} [*Swanson*, 1972], and $\Delta\rho = 700$ kg m^{-3}) and dividing by the area of the seimically active region (10 km^2 [*Ryan*, 1988]) yields a porosity of 10^{-7}, suggesting that there is sufficient energy available to cause the required melting and that we have even overestimated the heat transfer from the magma into the rock.

The effect of melting and thermomechanical erosion of fracture walls has been shown to be critical for the formation of discrete volcanoes. While we have demonstrated that there is in principle sufficient energy available for the melting process, more work is clearly needed on the general principle of magmatic erosion of lithospheric rock. Factors that have to be taken into account include chemistry (such as refractory phases in the mantle lithosphere and volatiles in the melt), the temperature evolution of the melt and the surrounding rock, and the rheology of the country rock at elevated temperatures.

4.4. Volcano Patterns

It was demonstrated that small off-axis perturbations grow over time. If the magma source region is wide enough and if the magma pressure is strongly super-Gaussian in cross section, the volcano pattern eventually reaches a steady state in which any three adjacent volcanoes form an equilateral triangle. Such a pattern is indeed observed in the volcano positions of the Hawaiian islands. Other volcanoes, such as some older portions of the Hawaiian-Emperor seamounts or the Louisville chain are located in largely unperturbed single lines. The fact that these single lines remained stable over significant length scales (and timescales) suggests that the magma source region may have been very narrow. A narrow source region may be caused by a reduction in plume flux. Comparison of plume strength in the Hawaiian chain (as evidenced by both swell and ridge volume) [*Davies*, 1992] with locations of volcanic shields [*Vogt*, 1974] indicates that a single line of volcanoes formed when the plume flux was at a minimum (located near 162°W), while wider patterns occurred during the plume flux maxima (located near 157°W and 168°W). Moreover, the volume flux of the Louisville plume is believed to be lower than that of the Hawaiian plume [*Davies*, 1988; *Sleep*, 1990], supporting the correlation between plume flux and average width of the resulting volcanic pattern. In older parts of the chain, however, such correlation is not observed, as the wide volcanic pattern around Midway Island is not matched by indications of significantly increased plume flux. A possible explanation is that greater quantities of melt generated owing to increased plume flux do not necessarily imply a wider melting region. Alternatively, the volume of island production and the width of the volcanic pattern may vary with changes in lithospheric thickness due to increased melting as the plume is able to reach shallower levels under thin lithosphere; this effect would be most noticeable as the hotspot track crosses fracture zones [*Phipps Morgan et al.*, 1995]. Across a fracture zone, a wider pattern would thus be expected on the side of the younger, thinner plate where melting on average occurs at shallower levels and is thus more voluminous. In this case, the width of the volcanic pattern would correlate both with the size of the swell and the thickness of the lithosphere provided that the swell is of thermal origin [*Davies*, 1992]. On the other hand, if the swell is of compositional origin (i.e., the residue becomes more buoyant after melt removal) [*Phipps Morgan et al.*, 1995], then a strong correlation would be expected between the width of the volcanic pattern and the size of the swell, as the volume of the swell records the amount of melt that has been removed, regardless of the mechanism that causes changes in melting.

5. Conclusion

The model described in this paper is robust in that it generates discrete volcanoes over a wide range of parameters. A parameter study led to the following conclusions:

1. The positive feedback mechanism due to melting and erosion of the fracture walls is necessary for the formation of discrete volcanoes.

2. The physical processes examined in this study (the amount of conduit wall erosion; the resistance of fracture volume changes to changes in magma pressure, stresses, and energy inputs causing erosion; the magma pressure in the plume; the width of the melting region of the plume; and the strength of the lithosphere) combine to determine model results such as spacing of volcanoes, focusing of magma, and pattern of volcanic locations. The complex interaction of the processes does not allow us to deduce any functional relation between processes and results. However, it is found that the magnitude of the plume stress (combined with the tensile strength of the lithosphere) predominantly influences volcano spacing. The amount of conduit wall erosion is crucial in determining whether the model results in a continuous ridge or discrete volcanoes. The resistance of dike opening to stresses and erosion mostly controls the amount of magma focusing towards the center of a volcanic edifice. The horizontal extent of the melting region of the plume largely determines the resulting volcanic pattern.

3. The *ten Brink* [1991] estimate of spacing is based purely on lithospheric elastic thickness, while our model also includes plume overpressurization. A high plume stress tends to decrease the spacing. On the other hand, *ten Brink* [1991] predicts volcano formation at the position of zero flexural stress due to the previous volcano, neglecting the effects of the flexural bulge of the older massive volcanoes. Our model, which accounts for the flexural response due to all volcanic loads, thus predicts greater spacing (counteracting the effects of magma overpressurization). Indeed, the spacing tends to be irregular due to varying volcano sizes.

4. By precluding eruptions in the vicinity of an existing volcano, flexural stresses can focus the magma flow at the surface into a region of $\sim$10–20 km diameter (using a lithospheric elastic thickness of 35 km).

5. The model generates discrete volcanoes with a steady plume and constant melt supply as input. A reasonably homogeneous distribution of melt is required that is only slightly larger in diameter than the volcanic pattern that is formed at the surface.

6. Dual lines and other wide volcano patterns form for a wide range of parameters for a plateau-shaped plume stress. Single lines are fundamentally unstable for wide enough source regions and typically lead to dual lines as small initial perturbations grow over time. The observed sudden change in the recent Hawaiian chain (at ~8 Ma, just north of Kauai) from a single to a dual line, however, suggests a large perturbation. Melting regions wide enough to allow triple lines or wider form wide volcano patterns instantaneously, regardless of initial perturbation.

Appendix A: Physical Meaning of Stresses σ_o, σ_1, and σ_p

The effective compressive background stress of the lithosphere is made up of two different components: (1) the tensile strength of the lithospheric rock given by σ_1 in equation (6) and (2) the asthenospheric underpressurization with respect to the plume given by σ_o in equation (1). These two effects were combined in the nondimensional formulation into parameter c_5.

While there is no maximum value of parameter c_5 beyond which the results become unreasonable (as long as the plume amplitude c_3 is adjusted accordingly), there does exist a minimum value below which the far-field lithosphere becomes susceptible to flexural perturbations on the hotspot axis and eruptions occur at unreasonable distances from the hotspot or the lithosphere becomes permeable everywhere leading to instability of the model. The value of c_5 chosen to generate the results shown is near this minimum value.

Redimensionalizing c_5 using a lithospheric thickness of 35 km, the total background stress ($\sigma_o + \sigma_1$) is 5.7×10^7 Pa, a reasonable value of tensile strength of lithospheric rock at depth. However, magma transport through the lithosphere is assumed to be via fractures which concentrate opening stresses at the tip. The effective tensile strength of the rock experienced by the fractures is thus reduced by a factor equal to the stress concentration at the fracture tips relative to the applied tensile stress. This factor depends on the type of nonlinear deformation occurring at the fracture tip but may be orders of magnitude [*Lister*, 1990; *Rubin*, 1995]; in linear elastic fracture mechanics this factor is infinite [*Rubin*, 1995]. The tensile strength is thus negligible with respect to other stresses. Hence it must be the asthenospheric underpressurization σ_o that contributes predominantly to the total background stress.

Viscous head loss describes an effective dynamic pressure drop in a porous medium due to high viscosity of the fluid. Both the asthenosphere and the magma-bearing plume material are forced into the overlying porous lithosphere by overpressurization. The high viscosity of the asthenosphere ($\sim 10^{18}$ Pa s) compared to that of the magma (~100 Pa s) results in a sufficiently large viscous head loss to make the lithosphere impermeable to asthenospheric material. The plume itself is not significantly pressurized with respect to the surrounding asthenosphere, but the viscous head loss there is essentially zero due to the presence of low-viscosity melt. Since most of the model runs yielding realistic results use a maximum plume stress ($\sigma_p - \sigma_1$) near zero, surrounded by high negative stress or pressure ($-\sigma_o - \sigma_1$), an interpretation of the stresses in terms of viscosities seems plausible.

Interpretation of the background stress as an effective pressure due to viscous head loss explains why there is no significant flexure due to the plume stresses (aside from the swell which covers a much greater area). If the plume stress of 5.7×10^7 Pa was either a fluid pressure or a traction due to plume deflection, significant flexure would be expected. The effective pressure due to viscous head loss does not cause flexure because it merely reflects different viscosities, while the pressure at the base of the lithosphere is constant and given by the overburden.

Acknowledgments. We thank Peter Olson and David Yuen for helpful reviews which greatly improved the manuscript.

References

Bargar, K. E., and E. D. Jackson, Calculated volumes of individual shield volcanoes along the Hawaiian-Emperor chain, *J. Res. U.S. Geol. Surv., 2*, 545–550, 1974.

Biot, M. A., General theory of three-dimensional consolidation, *J. Appl. Phys., 12*, 155–164, 1941.

Bonatti, E., Not so hot "hot spots" in the oceanic mantle, *Science, 250*, 107–111, 1990.

Bruce, P. M., and H. E. Huppert, Solidification and melting along dykes by the laminar flow of basaltic magma, in *Magma Transport and Storage,* edited by M. P. Ryan, pp. 87–101, John Wiley, New York, 1990.

Burnham, C. W., The importance of volatile constituents, in *The Evolution of the Igneous Rocks*, edited by H. S. Yoder, pp. 439–482, Princeton Univ. Press, Princeton, N.J., 1979.

Canuto, C., M. Y. Hussaini, A. Quarteroni, and T. A. Zhang, *Spectral Methods in Fluid Dynamics*, 567 pp., Springer Verlag, New York, 1988.

Carmichael, I. S. E., J. Nicholls, F. J. Spera, B. J. Wood, and S. A. Nelson, High temperature properties of silicate liquids: Applications to the equilibrium and ascent of basic magma, *Philos. Trans R. Soc. London, Ser. A, 286,* 373–431, 1977.

Clague, D. A., R. T. Holcomb, J. M. Sinton, R. S. Detrick, and M. E. Torresan, Pliocene and pleistocene alkalic flood basalts on the seafloor north of the Hawaiian Islands, *Earth Planet. Sci. Lett., 98*, 175–191, 1990.

Connolly, J. A. D., and Y. Y. Podladchikov, Compaction-driven fluid flow in viscoelastic rock, *Geodin. Acta, 11*, 55–84, 1998.

Davies, G. F., Ocean bathymetry and mantle convection, 1, Large-scale flow and hotspots, *J. Geophys. Res., 93*, 10,467–10,480, 1988.

Davies, G. F., Temporal variation of the Hawaiian plume flux, *Earth Planet. Sci. Lett., 113*, 277–286, 1992.

Davies, G. F., Thermomechanical erosion of the lithosphere by mantle plumes, *J. Geophys. Res., 99*, 15,709–15,722, 1994.

Delaney, P. T., and D. D. Pollard, Solidification of basaltic magma during flow in a dike, *Am. J. Sci., 282,* 856–885, 1982.

Eiler, J. M., K. A. Farley, J. W. Valley, A. W. Hofmann, and E. M. Stolper, Oxygen isotope constraints on the sources of Hawaiian volcanism, *Earth Planet. Sci. Lett. 144*, 453–468, 1996.

Evans, B., and D. L. Kohlstedt, Rheology of rocks, in *Rock Physics and Phase Relations: A Handbook of Physical Constants, AGU*

Ref. Shelf, vol. 3, edited by T. J. Ahrens, AGU, pp. 148–165, Washington, D. C., 1995.

Guéguen, Y., and V. Palciauskas, *Introduction to the Physics of Rocks*, 294 pp., Princeton Univ. Press, Princeton, N. J., 1994.

Hauri, E. H., J. C. Lassiter, and D. J. DePaolo, Osmium isotope systematics of drilled lavas from Mauna Loa, Hawaii, *J. Geophys. Res., 101*, 11,793–11,806, 1996.

Helfrich, K. R., and J. A. Whitehead, Solitary waves on conduits of buoyant fluid in a more viscous fluid, *Geophys. Astrophys. Fluid Dyn., 51*, 35–52, 1990.

Henyey, F. S., and N. Pomphrey, Self-consistent elastic moduli of a cracked solid, *Geophys. Res. Lett., 9*, 903–906, 1982.

Hieronymus, C. F., and D. Bercovici, Discrete alternating hotspot islands formed by interaction of magma transport and lithospheric flexure, *Nature, 397*, 604–607, 1999.

Ito, G., D. Bercovici, and S. J. Martel, Magma transport in the lithosphere through interacting dikes (abstract), *Eos Trans. AGU, 79*(45), Fall Meet. Suppl., F1006, 1997.

Kelemen, P. B., and E. Aharonov, Periodic formation of magma fractures and generation of layered gabbros in the lower crust beneath oceanic spreading ridges, in *Faulting and Magmatism at Mid-Ocean Ridges*, edited by W. R. Buck et al., *Geophys. Monogr. Ser.*, vol. 106, pp. 267–289, AGU, Washington D. C., 1998.

Kohlstedt, D. L., B. Evans, and S. J. Mackwell, Strength of the lithosphere: Constraints imposed by laboratory experiments, *J. Geophys. Res., 100*, 17,587–17,602, 1995.

Lister, J. R., Buoyancy-driven fluid fracture: The effects of material toughness and low viscosity precursors, *J. Fluid. Mech., 210*, 263–280, 1990.

Lister, J. R., and P. J. Dellar, Solidification of pressure-driven flow in a finite rigid channel with application to volcanic eruptions, *J. Fluid Mech., 323*, 267–283, 1996.

Lister, J. R., and R. C. Kerr, Fluid-mechanical models of crack propagation and their application to magma transport in dykes, *J. Geophys. Res., 96*, 10,049–10,077, 1991.

Maaløe, S., Shape of ascending feeder dikes, and ascent modes of magma, *J. Volcanol. Geotherm. Res., 81*, 207–214, 1998.

Marsh, B. D., On the cooling of ascending andesitic magma, *Philos. Trans. R. Soc. London, Ser. A, 288*, 611–625, 1978.

McGovern, P. J., and S. C. Solomon, Finite element models of flank deformation and stresses in large volcanoes (abstract), *Eos Trans. AGU, 74*(43), Fall Meet. Suppl., 646–647, 1993.

McGovern, P. J., and S. C. Solomon, Filling of flexural moats around large volcanoes on Venus: Implications for volcano structure and global magmatic flux, *J. Geophys. Res., 102*, 16,303–16,318, 1997.

Muller, J., Topographic and gravitational stresses: Effects on translational landslide rupture surface growth and the propagation of dikes beneath volcanoes, M.S. thesis, Univ. of Hawaii at Manoa, Honolulu, 1999.

Nadai, A., *Theory of Flow and Fracture of Solids*, 348 pp., McGraw-Hill, New York, 1963.

Olson, P., and U. Christensen, Solitary wave propagation in a fluid conduit within a viscous matrix, *J. Geophys. Res., 91*, 6367–6374, 1986.

Olson, P., and H. Singer, Creeping plumes, *J. Fluid Mech., 158*, 511–531, 1985.

Phipps Morgan, J., W. J. Morgan, and E. Price, Hotspot melting generates both hotspot volcanism and a hotspot swell?, *J. Geophys. Res., 100*, 8045–8062, 1995.

Rubin, A. M., Propagation of magma-filled cracks, *Annu. Rev. Earth Planet. Sci., 23*, 287–336, 1995.

Ryan, M. P., The mechanics and three-dimensional internal structure of active magmatic systems: Kilauea volcano, Hawaii, *J. Geophys. Res., 95*, 4213–4248, 1988.

Schmalholz, S. M., and Y. Y. Podladchikov, Buckling versus folding: Importance of viscoelasticity, *Geophys. Res. Lett., 26*, 2641–2644, 1999.

Schubert, G., P. Olson, C. Anderson, and P. Goldman, Solitary waves in mantle plumes, *J. Geophys. Res., 94*, 9523–9532, 1989.

Scott, D. R., D. J. Stevenson, and J. A. Whitehead, Observations of solitary waves in a viscously deformable pipe, *Nature, 319*, 759–760, 1986.

Skilbeck, J. N., and J. A. Whitehead, Formation of discrete islands in linear island chains, *Nature, 272*, 499–501, 1978.

Sleep, N. H., Hotspots and mantle plumes: Some phenomenology, *J. Geophys. Res., 95*, 6715–6736, 1990.

Spence, D. A., and D. L. Turcotte, Magma-driven propagation of cracks, *J. Geophys. Res., 90*, 575–580, 1985.

Spence, D. A., P. W. Sharp, and D. L. Turcotte, Buoyancy-driven crack propagation: A mechanism for magma migration, *J. Fluid. Mech., 174*, 135–153, 1987.

Spera, F. J., Aspects of Magma Transport, in *Physics of Magmatic Processes*, edited by R. B. Hargraves, pp. 265–323, Princeton Univ. Press, Princeton, N. J., 1980.

Stevenson, D. J., Migration of fluid-filled cracks: Applications to terrestrial and icy bodies, *Lunar Planet. Sci. Conf., 13*, 768–769, 1982.

Swanson, D. A., Magma supply rate at Kilauea volcano, 1952–1971, *Science, 175*, 169–170, 1972.

ten Brink, U., Volcano spacing and plate rigidity, *Geology, 19*, 397–400, 1991.

Timoshenko, S., and S. Woinowsky-Krieger, *Theory of Plates and Shells*, 580 pp., McGraw-Hill, New York, 1959.

Turcotte, D. L., Some thermal problems associated with magma migration, *J. Volcanol. Geotherm. Res., 10*, 267–278, 1981.

Turcotte, D. L., Magma migration, *Annu. Rev. Earth Planet. Sci., 10*, 397–408, 1982.

Turcotte, D. L., and G. Schubert, *Geodynamic Applications of Continuum Physics to Geological Problems*, 450 pp., John Wiley, New York, 1982.

Vogt, P. R., Volcano spacing, fractures, and thickness of the lithosphere, *Earth Planet. Sci. Lett., 21*, 235–252, 1974.

Wessel, P., Observational constraints on models of the Hawaiian hot spot swell, *J. Geophys. Res., 98*, 16,095–16,104, 1993.

Whitehead, J. A., Jr., Instabilities of fluid conduits in a flowing Earth—are plates lubricated by the asthenosphere?, *Geophys. J. R. Astron. Soc., 70*, 415–433, 1982.

D. Bercovici, Department of Geology and Geophysics, University of Hawaii at Manoa, Honolulu, HI 96822. (dberco@soest.hawaii.edu)

C. Hieronymus, Danish Lithosphere Centre, Øster Voldgade 10 L, 1350 Copenhagen K, Denmark. (cfh@dlc.ku.dk)

(Received February 28, 2000; revised September 8, 2000; accepted September 25, 2000.)